WL-TR- **97-3044**

IMPLEMENTATION OF A DAMAGE TOLERANCE MODULE INTO ASTROS

D.S. PIPKINS
S.N. ATLURI

Knowledge Systems, Inc.,
81 E. Main St.
Forsyth, GA 31029

APRIL 1996

FINAL REPORT FOR THE PERIOD SEPTEMBER 1995 - MARCH 1996

THIS IS A SMALL BUSINESS INNOVATION RESEARCH (SBIR) PHASE I REPORT

APPROVED FOR PUBLIC RELEASE; DISTRIBUTION IS UNLIMITED

FLIGHT DYNAMICS DIRECTORATE
WRIGHT LABORATORY
AIR FORCE MATERIEL COMMAND
WRIGHT-PATTERSON AIR FORCE BASE, OHIO 45433-7552

NOTICE

WHEN GOVERNMENT DRAWINGS, SPECIFICATIONS, OR OTHER DATA ARE USED FOR ANY PURPOSE OTHER THAN IN CONNECTION WITH A DEFINITE GOVERNMENT-RELATED PROCUREMENT, THE UNITED STATES GOVERNMENT INCURS NO RESPONSIBILITY OR ANY OBLIGATION WHATSOEVER. THE FACT THAT THE GOVERNMENT MAY HAVE FORMULATED OR IN ANY WAY SUPPLIED THE SAID DRAWING, SPECIFICATIONS OR OTHER DATA, IS NOT TO BE REGARDED BY IMPLICATION, OR OTHERWISE IN ANY MANNER CONSTRUED, AS LICENSING THE HOLDER, OR ANY OTHER PERSON OR CORPORATION; OR AS CONVEYING ANY RIGHTS OR PERMISSION TO MANUFACTURE, USE, OR SELL ANY PATENTED INVENTION THAT MAY IN ANY WAY BE RELATED THERETO.

THIS REPORT IS RELEASABLE TO THE NATIONAL TECHNICAL INFORMATION SERVICE (NTIS). AT NTIS, IT WILL BE AVAILABLE TO THE GENERAL PUBLIC, INCLUDING FOREIGN NATIONS.

THIS TECHNICAL REPORT HAS BEEN REVIEWED AND IS APPROVED FOR PUBLICATION.

Victoria A. Tischler
Project Engineer
Design and Analysis Branch

Peter M. Flick, Prinicpal Engineer
Design and Analysis Branch

Nelson Wolf, Acting Chief
Design and Analysis Branch
Structures Division

IF YOU ADDRESS HAS CHANGED, IF YOU WISH TO BE REMOVED FROM OUR MAILING LIST, OR IF THE ADDRESSEE IS NO LONGER EMPLOYED BY YOUR ORGANIZATION, PLEASE NOTIFY WL/FIBD BLDG 45, 2130 EIGHTH STREET, SUITE 1, WRIGHT-PATTERSON AFB OH 45433-7552 TO HELP MAINTAIN A CURRENT MAILING LIST.

Copies of this report should not be returned unless return is required by security considerations, contractual obligations, or notice on a specified document.

REPORT DOCUMENTATION PAGE

Form Approved
OMB No. 0704-0188

1. AGENCY USE ONLY (Leave blank)	2. REPORT DATE	3. REPORT TYPE AND DATES COVERED
	APR 1996	FINAL 09/29/95 – 04/29/96

4. TITLE AND SUBTITLE

Implementation of a Damage Tolerance Module into ASTROS

5. FUNDING NUMBERS

C F33615-95-C-3226
PE 65502
PR 3005
TA 41
WU 38

6. AUTHOR(S)

D.S. Pipkins and S.N. Atluri

7. PERFORMING ORGANIZATION NAME(S) AND ADDRESS(ES)

Knowledge Systems, Inc.
81 East Main Street
Forsyth, GA 31029-1828

8. PERFORMING ORGANIZATION REPORT NUMBER

9. SPONSORING/MONITORING AGENCY NAME(S) AND ADDRESS(ES)

FLIGHT DYNAMICS DIRECTORATE
WRIGHT LABORATORY
AIR FORCE MATERIEL COMMAND
WRIGHT PATTERSON AFB OH 45433-7562
POC: VICTORIA A. TISCHLER, WL/FIBD (937) 255-6992

10. SPONSORING/MONITORING AGENCY REPORT NUMBER

WL-TR-97-3044

11. SUPPLEMENTARY NOTES THIS IS A SMALL BUSINESS INNOVATION RESEARCH (SBIR) PHASE I REPORT.

12a. DISTRIBUTION/AVAILABILITY STATEMENT

APPROVED FOR PUBLIC RELEASE; DISTRIBUTION IS UNLIMITED.

12b. DISTRIBUTION CODE

13. ABSTRACT *(Maximum 200 words)*

This report discusses the implementation of a damage tolerance module into the multidisciplinary analysis and design software, ASTROS. The module will make use of state of the art, computationally efficient algorithms for determining the residual strength and life of metallic and composite structures with damage. The damage tolerance module will enhance the existing capabilities of ASTROS by allowing constraints based on damage tolerance requirements to be considered simultaneously with those based on strength, stiffness, aeroelastic response, etc.

14. SUBJECT TERMS

ASTROS, COMPOSITE, DELAMINATION,BUCKLING, DAMAGE TOLERANCE, FRACTURE, FATIGUE

15. NUMBER OF PAGES 46

16. PRICE CODE

17. SECURITY CLASSIFICATION OF REPORT	18. SECURITY CLASSIFICATION OF THIS PAGE	19. SECURITY CLASSIFICATION OF ABSTRACT	20. LIMITATION OF ABSTRACT
UNCLASSIFIED	UNCLASSIFIED	UNCLASSIFIED	SAR

NSN 7540-01-280-5500

Standard Form 298 (Rev. 2-89)
Prescribed by ANSI Std. Z39-18
298-102

Contents

List of Figures

1 Introduction

In addition to requirements such as strength, stiffness, and aeroelastic response it is necessary to design both metallic and composite aircraft structures to withstand the effects of damage. By doing so, safe, economical fleets with high operational readiness can be insured. The importance of safety and operational readiness to profitability and competitiveness in a commercial aviation setting and national defense in a military one is apparent. To insure that metallic aircraft structures are designed and maintained to withstand the effects of damage, the Federal Aviation Administration (FAA) and United States Air Force (USAF) have established specific guidelines which must be followed. The FAA requires commercial transport aircraft certified under part 25 of the Federal Aviation Regulations (FAR) to meet certain Damage Tolerance Requirements (DTR). Similarly, the USAF has specified a set of DTR for metallic structures which are described in detail in MIL-STD-1530A. For composite structures, the FAA does not have formal requirements for certification at this time. The Air Force, on the other hand, has specified a set of DTR for composite structures in AFGS-87221A. The DTR, as set forth by both the FAA and the Air Force, essentially state that:

- the residual strength of an airframe structural component shall not drop below that required to sustain limit load, and
- that inspections must be scheduled to insure that the required level of residual strength is maintained.

The primary means by which the DTR are satisfied by commercial and military airframe manufacturers and maintenance organizations is through the performance of a Damage Tolerance Assessment (DTA). The DTA involves the development of damage growth curves and residual strength diagrams for individual structural components of an airframe. This allows the residual strength as a function of aircraft usage to be determined. With this information, manufacturers can design components which minimize the evolution and growth of damage and its effect on the integrity of the aircraft structure. Further, appropriate inspection intervals can be specified which insure that the structural integrity of the aircraft will be maintained through out its life.

At present, there is no software which integrates damage tolerance with the other disciplines (i.e. strength, stiffness, aeroelastic response, etc.) which impact the design of an aircraft structure. As a result, the design of an aircraft structure which satisfies damage tolerance requirements in addition to those of other disciplines, is presently accomplished via a manual "cut and try" procedure. This type of design process is time consuming and therefore very costly [Nees (1995)]. To address this deficiency in existing software, this SBIR project is implementing a damage tolerance module into the multidisciplinary analysis and design software, ASTROS.

Phase I of this SBIR project has addressed the damage tolerance analysis of aircraft structures made of laminated composites. The damage considered was in the form of a delamination between lamina in a stiffened panel. The Phase I effort accomplished the following.

- A damage tolerance software applicable to laminated composites, called BUCKDEL, was developed. The BUCKDEL software, performs geometrically nonlinear analysis of stiffened laminated composite plates with and without delaminations. BUCKDEL allows the user to perform: a linear static solution; a linear buckling (eigenvalue) analysis; and a nonlinear post-buckling analysis through both limit and bifurcation points. BUCKDEL also calculates the pointwise energy release rates around a delamination front using an Equivalent Domain Integral (EDI) technique. The energy release rates can be used to predict the growth and onset of unstable propagation of a delamination.

- The feasibility of using a global-local approach to link an ASTROS finite element analysis (global) with a local damage analysis (such as that performed by BUCKDEL) was investigated. This global-local approach was found to be workable, due in large part to the ASTROS system architecture which allows the user to introduce special purpose modules by making use of the SYSGEN program which is provided with ASTROS.

Based on the Phase I results, the implementation of a damage tolerance module into ASTROS which accounts for typical damage in both composite and metallic structure is feasible. The remainder of this report will describe how the implementation of the damage tolerance module will be carried out. In addition, Users and Theory Manuals for BUCKDEL are included with this report. The BUCKDEL software represents a component of the damage tolerance module.

2 SBIR Technical Objectives

The objective of this SBIR project is to develop damage tolerance software which can be used in a 'stand alone' mode or as an analysis module in the multidisciplinary analysis and design software, ASTROS. The software will use state of the art, computationally efficient algorithms for determining the residual strength and life [Atluri (1995)] of metallic and composite structures with damage. When used as an analysis module, it will enhance the existing capabilities of ASTROS by allowing constraints based on damage tolerance requirements to be considered simultaneously with those based on strength, stiffness, aeroelastic response, etc. during design optimization. Included in potential commercial applications of such a capability are industries involved in the design of aircraft structures, automobiles, bridges and buildings.

ASTROS is well suited for modeling global strength, stiffness, and aeroelastic response of undamaged, stiffened structure. However, it presently does not have the capability to account for local damage such as cracks, delaminations, and penetration holes. Therefore, this SBIR project will:

- utilize ASTROS existing capabilities for performing global level modeling of the structure;

- utilize an existing loads program called USAGE [Nees (1995)] to general load spectra in terms of ASTROS load cases;
- develop a finite element based damage tolerance module to model local damage in metallic and composite materials;
- develop interface software to facilitate the linking of ASTROS with the damage tolerance module via the SYSGEN program and a modified MAPOL sequence.
- define new bulk data entries, relational schema and error messages needed to integrate the damage tolerance module with ASTROS.

To supplement the finite element based damage tolerance module, the SBIR project will also develop 'look up' tables containing cataloged solutions (i.e. stress intensity factors, energy release rates, etc.), which can be used to obtain estimates of the residual strength and life of common structural geometries. In addition to saving computational time, these 'look up' tables can be used to provide sanity checks on the finite element calculations.

The damage scenarios that will be considered in the damage tolerance module are:

- single or multiple skin cracks (Widespread Fatigue Damage) in a stiffened structure, including the effect of broken stiffeners (Fig. 1)[tensile loading, metallic and composite materials];
- skin crack turning at stiffeners and its effect on fail safety [tensile loading, metallic and composite materials];
- single or multiple part elliptical surface flaws at holes or other stress raisers (Fig. 2) [tensile loading; metallic materials]
- arbitrary shaped holes (Fig. 3)[compressive loading, metallic and composite materials]; and
- arbitrary shaped delaminations (Fig. 4)[compressive loading, composite materials].

For each damage scenario, the ability to calculate the residual strength of a structure containing that type of damage will be provided in the damage tolerance module. A residual life (fatigue) capability will be provided for elliptical surface flaws and skin cracks which propagate in a self similar manner. The damage tolerance module will also evaluate DTR imposed design constraints and constraint sensitivities for use by the optimization routine in ASTROS.

For metallic or composite aircraft structure loaded in tension, the damage of principal interest during design is usually in the form of cracks normal to the direction of principal tension. These cracks typically occur over time due to fatigue or suddenly due to an event such as an uncontained failure of a rotating engine component or battle damage. A crack arising suddenly due to a catastrophic event is an example of discrete source damage (DSD).

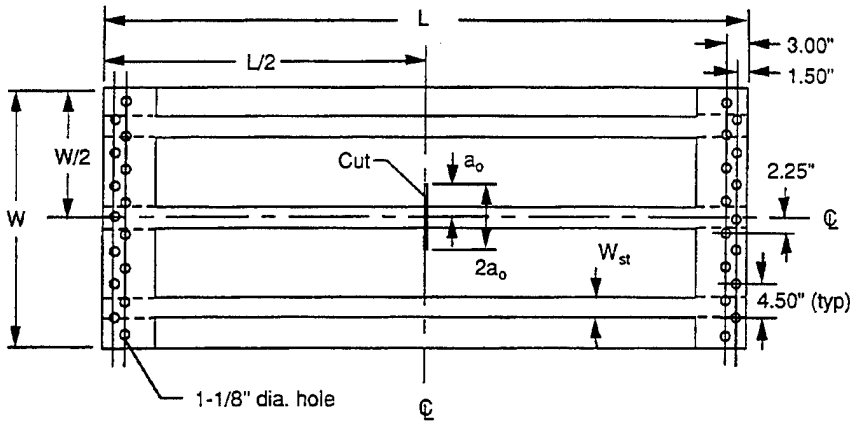

Figure 1: Central Crack and Broken Stiffener in a Panel

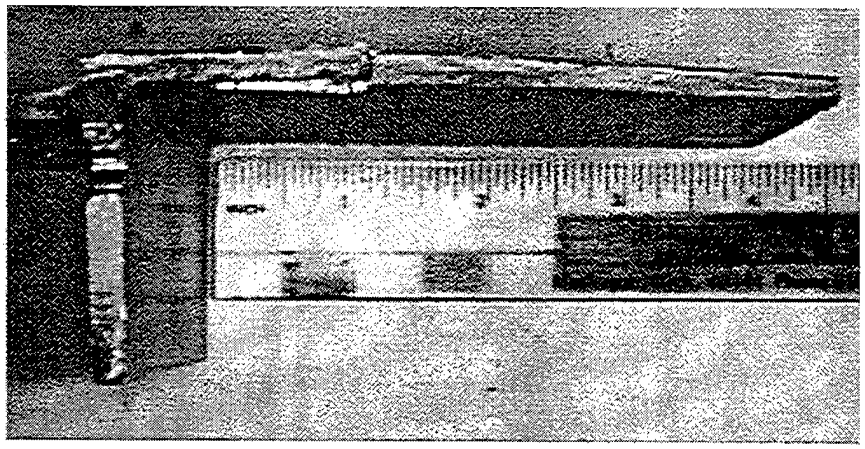

Figure 2: Failed Lower Wing Panel of a U.S. Air Force C-141B Due to the Growth of a Surface Flaw

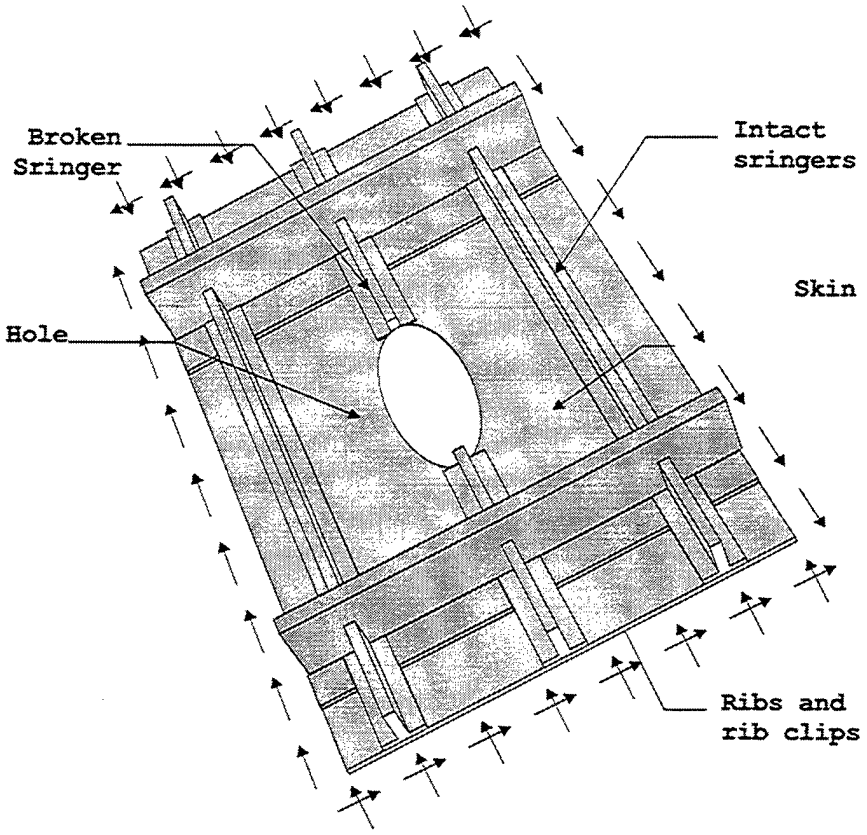

Figure 3: Hole in the Upper (Compression) Skin of a Wing

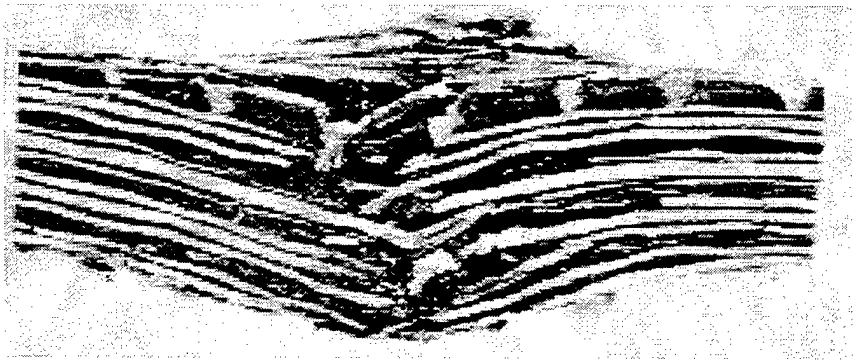

Figure 4: Delamination Due to Impact of a Laminated Composite

In reality, DSD in a structure loaded in tension such as a fuselage or lower wing would be in the form of an irregular shaped hole. However, since a crack of length 'a' is more critical than a hole of diameter 'a', the crack representation of DSD represents a worst case scenario. Therefore, for reasons of conservatism and practicality (both experimental and analytical) the crack is used in the certification of primary structural elements loaded in tension. Residual strength and life calculations for structure containing cracks and loaded in tension will be based on Linear Elastic Fracture Mechanics (LEFM). Thus, the parts of the damage tolerance module which address cracked structure will compute stress intensity factors and their sensitivities to changes in the design variables. These values can then be used to evaluate constraints based on residual strength requirements. For constraints based on residual life (fatigue) requirements, computed stress intensity factors will be used in crack growth equations to determine the time required for a crack or cracks to grow to a critical size. The critical size is determined from a residual strength requirement such as that requiring the structure to be able to sustain limit load at any time in its life.

For metallic or composite aircraft structure loaded in compression, the primary concern is with DSD in the form of a hole or crack parallel to the direction of principal compression. For laminated composites, delaminations between lamina are also of concern. Delaminations can result from excessive interlaminar shear stresses or through-the-thickness tensile stresses at holes, free edges, section changes, or in bonded joints; panel buckling; and low velocity impact. The modeling of delaminations in laminated composites was addressed in Phase I and resulted in the development of the BUCKDEL software. The residual strength of structure loaded in compression will be based on the buckling and post-buckling behavior of the structure. For laminated composites containing delaminations, the pointwise energy release rate around the delamination front will also be used in the residual strength prediction.

The motivation for modeling DSD in a structure loaded in compression in the form of a hole or crack parallel to the direction of principal compression is as follows. For a stiffened structure, the buckling load is expected to vary significantly with the size, shape (i.e. circular or elliptical), and location (i.e. distance from the wing tip) of the hole. Some results reported in the literature [Vellaichamy et. al (1990), Nemeth (1990), and Britt (1994)] indicate, as is to be expected, that for an elliptical hole with the major axis along the direction of compression, the initial buckling load is lower than that for a circular hole of the same area. Similarly, if a panel is subject to pure shear in the x-y plane, the shear buckling load will be minimum when the major axis of the ellipse is at 45 degrees to the x axis. The buckling load will decrease with an increase in the aspect ratio of the ellipse. The most severe case being in the limit when the ellipse degenerates into a crack (with the crack axis along the direction parallel to the direction of compression). Based upon this discussion, it is anticipated that the worst case DSD scenario for primary structure loaded in compression will be a crack oriented such that its axis is parallel to the direction of maximum compressive stress.

3 Implementation of the Damage Tolerance Module

3.1 Damage Tolerance Analysis of Stiffened Structure, Using a Global-Local Methodology

The method for calculating the residual strength and life of a stiffened structure made of metallic and/or composite materials is to use a global-local methodology. The global analysis will be accomplished via ASTROS while the damage tolerance module will be used for the local analysis. To illustrate this methodology, consider the case of a wing containing a crack in the skin of the lower surface [Fig. 5]. (Note that the methodology is general in nature and can be used for structure containing damage in the form of penetration holes and/or delaminations.) A coarse finite element mesh is first used to model the global behavior of the cracked wing. The traction and/or displacement boundary conditions to be applied to the local model are determined from the results of the global analysis. These boundary conditions include the reaction forces, exerted by the stringers and ribs, on the skin. The Finite Element Alternating Method (FEAM) is used in the local analysis to determine the stress intensity factors. The FEAM allows a coarse finite element mesh to be used for the local model of the skin because the crack tip fields are captured by an analytical solution and thus cracks need not be modeled explicitly in the mesh. The FEAM along with the other local damage modeling methodologies to be implemented in the damage tolerance module will be discussed in detail in later sections.

In the global analysis, the stringers are modeled as beams (ASTROS CBAR elements) attached to the skin (ASTROS CQUAD4 or CTRIA3 elements), and ribs are modeled as plates (ASTROS CQUAD4 or CTRIA3 elements) or shear panels (ASTROS CSHEAR elements), as illustrated in Fig. 6. To account for fastener flexibility, springs (ASTROS CELAS1 or CELAS2 element) can be used to model connections between stiffening elements and the skin. This level of detail in the global model should be sufficient for most situations. However, the user is free to either decrease or increase the complexity of the global model, within the limits imposed by the modeling capabilities of ASTROS.

Damage in the form of delaminations typically need not be accounted for in the global model. On the other hand, damage in the form of cracks or penetration holes does need to be accounted for if it is of sufficient size to affect load transfer in the structure. To accomplish this, holes are modeled explicitly (as holes) while cracks are modeled via unconnected nodes at the crack locations. This crude representation of the crack in the global model reflects the loss of stiffness in the structure, so that the redistribution of loads among the skin, stringers and ribs can be captured. Broken stringers and ribs, if any, are also accounted for in a similar manner. The details of the crack tip fields are ignored at this level of analysis. The global analysis results are used to construct a free-body diagram (Fig. 7) of the cracked sheet (local model), with the applied loading on the sheet being the reaction forces from stringers and ribs as well as the loading on the periphery of the sheet.

For problems involving fatigue where the crack is of sufficient size that it must be accounted for in the globlal model, it will be necessary to update the crack size periodically.

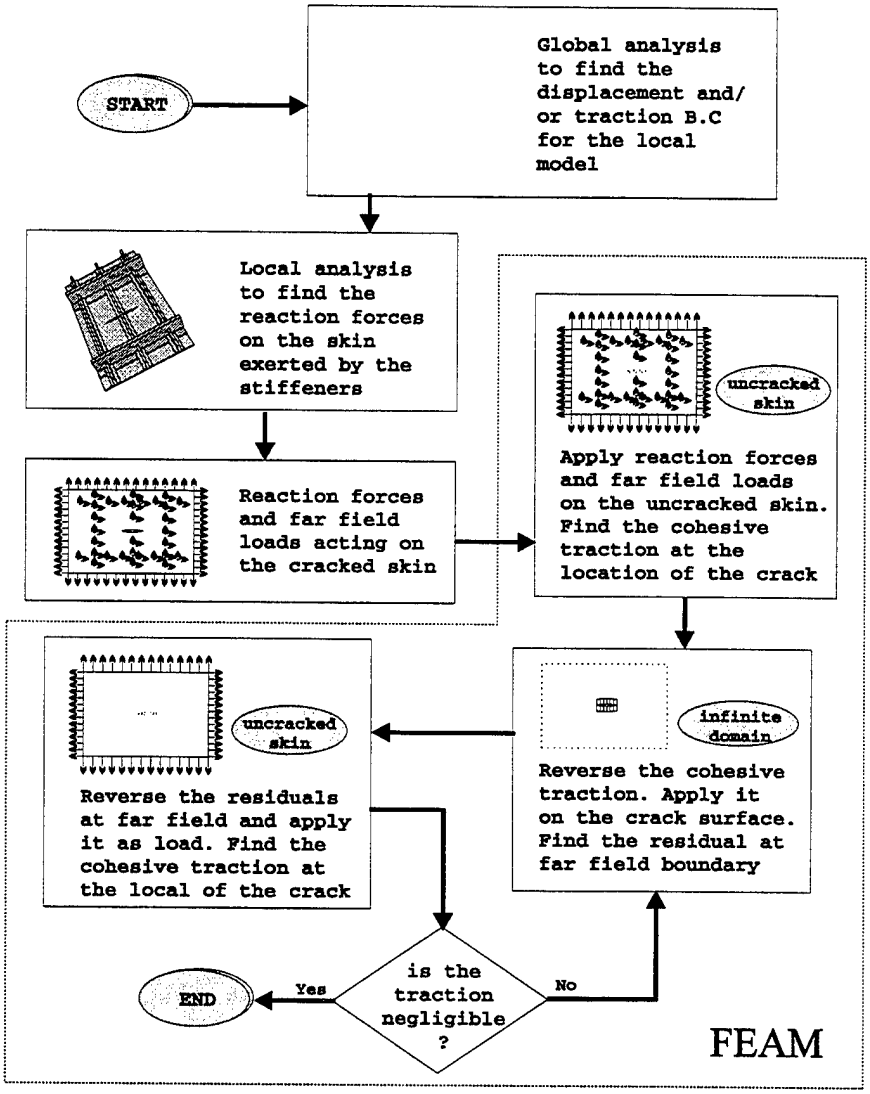

Figure 5: Flow Chart Illustrating the Damage Tolerance Analysis of a Wing Using a Global-Local Methodology

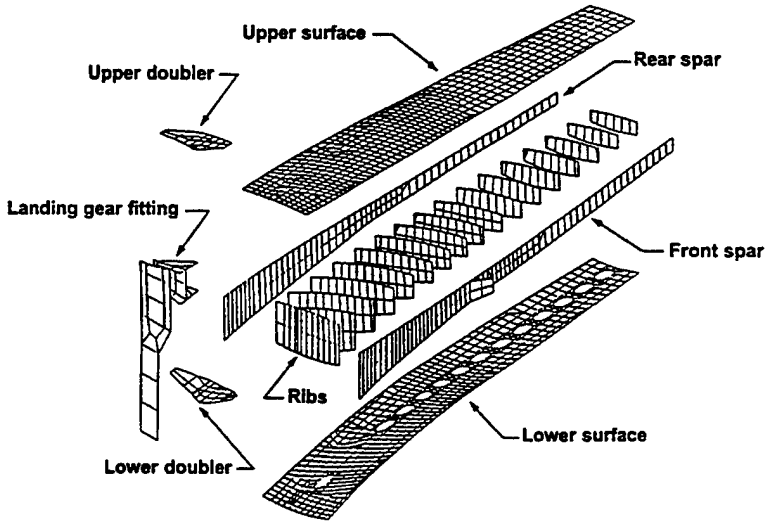

Figure 6: A Global Analysis

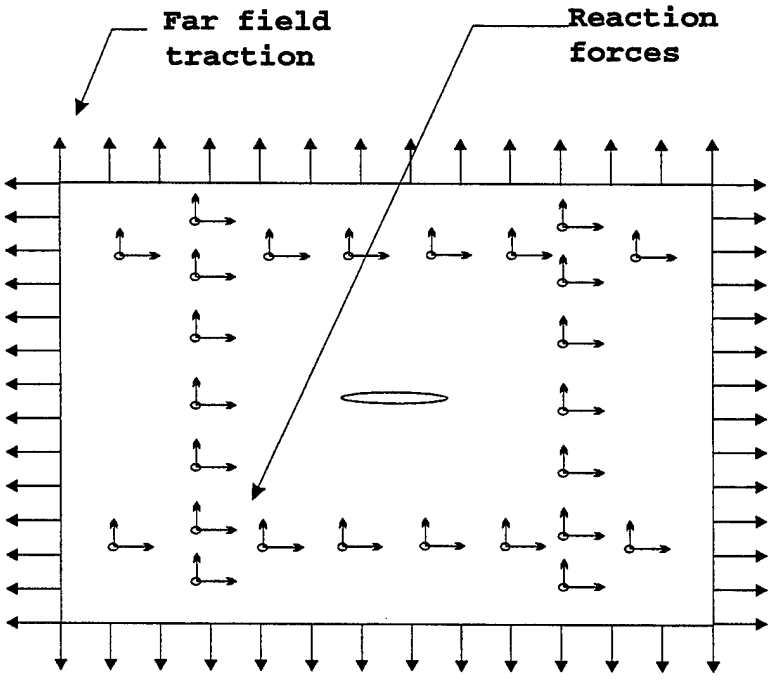

Figure 7: The Isolated Skin (Local Model)

This will allow changes in the load distribution to be determined and the boundary conditions applied to the local model to be updated. In general, the same global model can be used for a number of local analyses. The SBIR project will automate this updating of crack size in the global model.

During the course of the Phase I project, the possibility of using an intermediate analysis between the global and local analysis was considered. The intermediate analysis would provide an additional level of detail which in some cases, may improve the fidelity of the local boundary conditions. The global-local approach was settled upon over the global-intermediate-local approach for two reasons. First, since ASTROS is primarily a preliminary design tool, the geometric details required to do the finite element modeling of stiffeners and fasteners at the intermediate level may not be available at this design phase. Second, the additional computational burden imposed by the intermediate analysis would likely slow down the ASTROS iterative design process. This would be of particular concern during the design of a structure such as a wing in which damage related constraints were being considered in multiple panels.

3.2 Damage Tolerance Module

The finite element based damage tolerance module for modeling local damage will implement the following computational methods:

- Finite Element Alternating Method [Wang and Atluri (1996)] for modeling single or multiple cracks (including Widespread Fatigue Damage) under tension loading;
- hybrid crack-tip finite elements [Atluri (1986)] for modeling single or multiple cracks under tension loading and crack turning at a stiffener;
- Finite Element Alternating Method for modeling single or multiple part elliptical surface flaws at holes or other stress raisers [Nishioka and Atluri (1983)]; and
- a multi-domain modeling method (implemented in BUCKDEL during Phase I) for calculating the buckling and post-buckling strengths of stiffened panels with arbitrary shaped holes and/or delaminations.

This module, when combined with ASTROS will provide a global-local methodology for modeling damage in a complex stiffened structure. This will allow residual strength and residual life (fatigue) constraints stemming from the DTR to be treated by ASTROS during multidisciplinary design and optimization. In addition to finite element based damage modeling, 'look up' tables containing cataloged solutions will provide a means of treating problems involving common geometries as efficiently as possible as well as a convenient way of checking the finite element calculations.

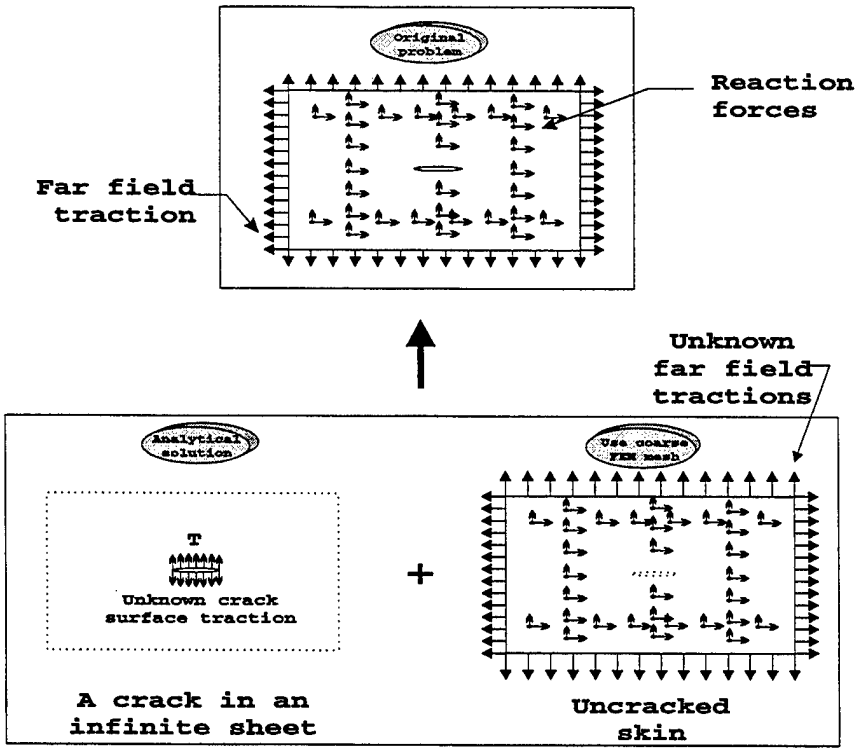

Figure 8: Superposition Principle Used in the Finite Element Alternating Method

3.2.1 Finite Element Alternating Method For Modeling Single or Multiple Cracks: Tensile Loading

Once the global analysis is performed with ASTROS, one can consider the free-body diagram of the cracked skin alone (see Fig. 7); the skin being subjected to far-field tractions, and the stiffener reaction forces. The stress-intensity factors for single or multiple cracks (including Widespread Fatigue Damage) in the skin can be determined in the local analysis using the Finite Element Alternating Method (FEAM), while still using a coarse finite element mesh. The problem in Fig. 7 can be solved with the FEAM depicted in Fig. 8, wherein it can be seen that the problem of Fig. 7, can be identified with the problem labeled as the "original problem" in Fig. 8.

The FEAM is based on the Schwartz-Neumann alternating method (see the Appendix for theoretical details). The combination of the powerful finite element method, and the analytical solutions for cracks in an infinite domain, subjected to *arbitrary* crack surface tractions (that have only recently been developed), enable the alternating method to be used to solve fracture problems for complex structures. With the help of the initial stress method, it can even be used in elastoplastic analyses [Wang, Brust and Atluri (1995a), (1995b), and (1995c)]. It has been used successfully in the evaluation of residual strength and life of cracked metallic and composite structures. The Finite Element Alternating Method solves the problem of cracks in finite bodies by iterating between the analytical solution for an

embedded crack in an infinite domain, and the finite element solution for the uncracked finite skin. Essentially, it is a fixed point iteration scheme which solves the superposition of the following two problems[see Fig. 8].

1. the uncracked, finite-sized skin subjected to external loads (including the reaction forces exerted by the stiffeners on the skin) and unknown external boundary loads;
2. a crack in an infinite sheet subjected to a crack surface traction

The crack surface traction in the infinite sheet cancels out the cohesive traction at the location of the crack in the first problem; while the unknown external boundary loads in the first problem cancel out the tractions at the same location in the second problem. Thus, the original problem, i.e. a cracked sheet of a finite dimension subjected to reaction forces exerted by the stiffeners with other boundary loadings, is exactly the superposition of these two problems.

The FEAM is used to solve this superposition problem. First, reverse the cohesive tractions at the location of the crack in the finite element model of the uncracked skin and use them as the load acting on the crack in an infinite sheet. Then, reverse the residuals at the locations of the far field boundries in the infinite sheet and apply them as loads acting on the boundaries of the uncracked skin. In this way, the cohesive tractions at the location of cracks and residuals at the locations of the external boundaries are corrected iteratively. This procedure converges very fast, usually in two or three iterations. A flow chart illustrating the FEAM is shown in Fig. 9.

Fracture mechanics parameters can be found accurately because the near crack tip fields are captured exactly by the analytical solutions. Coarser meshes can be used in the finite element analysis because the cracks are not modeled explicitly. The finite element method is only used to compute the cohesive tractions at the crack location, which has a smooth distribution. Therefore, a very coarse mesh can be used. Fig. 10 shows the typical finite element meshes around the crack tip, when a) the Equivalent Domain Integral (EDI) based method is used to evaluate stress intensity factors; or, b) the FEAM is used. In Fig. 10, the EDI based method also uses singular quarter-point elements. The simplicity of the FEAM mesh relative to the EDI mesh, which must explicitly model crack tips is apparent from this figure.

In a parametric analysis of various crack sizes, such as is necessary in fatigue calculations, the stiffness matrix of the finite element model is decomposed only once, since the stiffness of the uncracked structure remains the same for all crack sizes. In the other approaches, such as those using singular/hybrid type special crack-tip finite elements or EDI methods, the cracks must be modeled explicitly. Therefore, the global stiffness matrix must be computed and decomposed for each crack size. Thus, the FEAM is very efficient in terms of both computational time and human effort (i.e. mesh generation) when applied to problems such as fatigue crack growth.

Finally, it is noted that a simple superposition method can be used to construct the solution for multiple cracks in an infinite domain, subjected to arbitrary crack surface tractions,

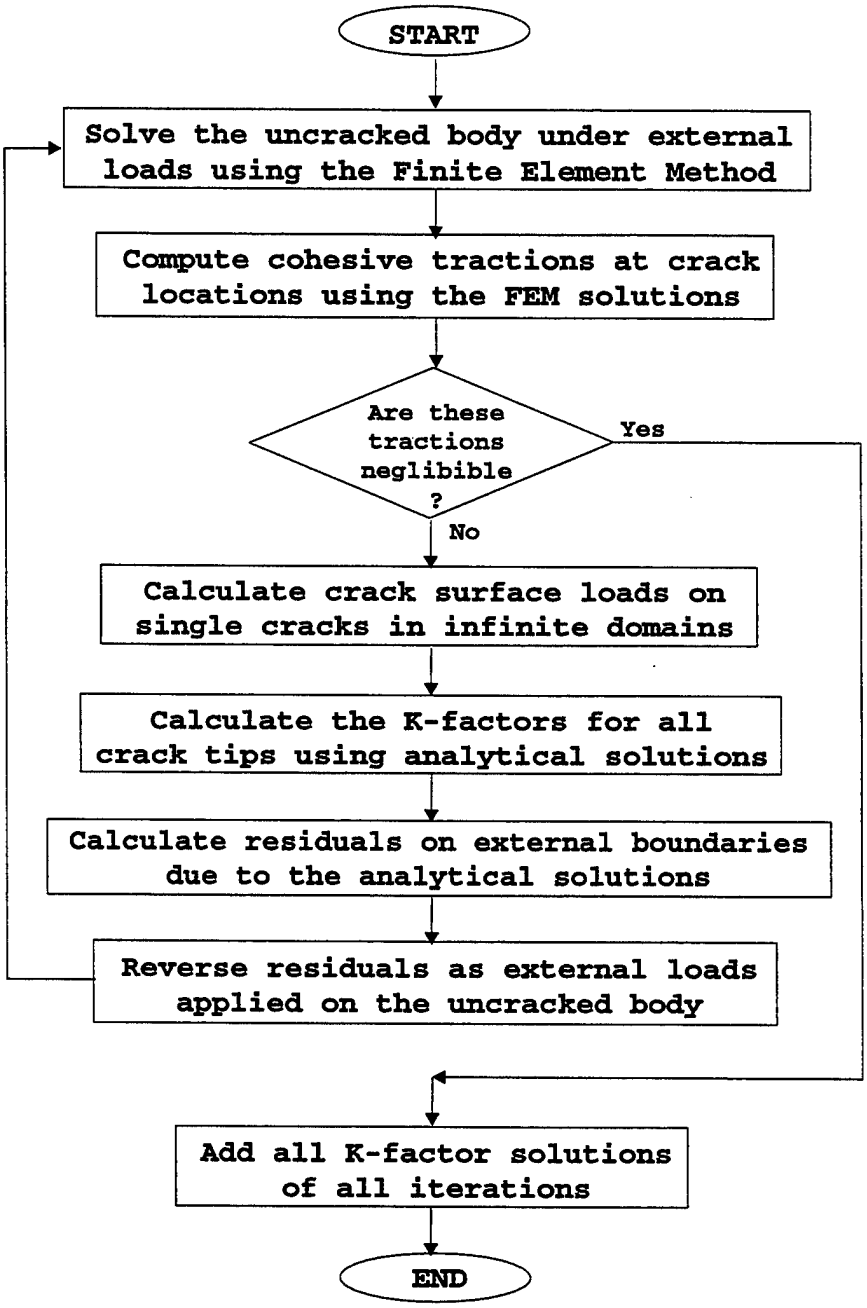

Figure 9: Flow Chart of the Finite Element Alternating Method

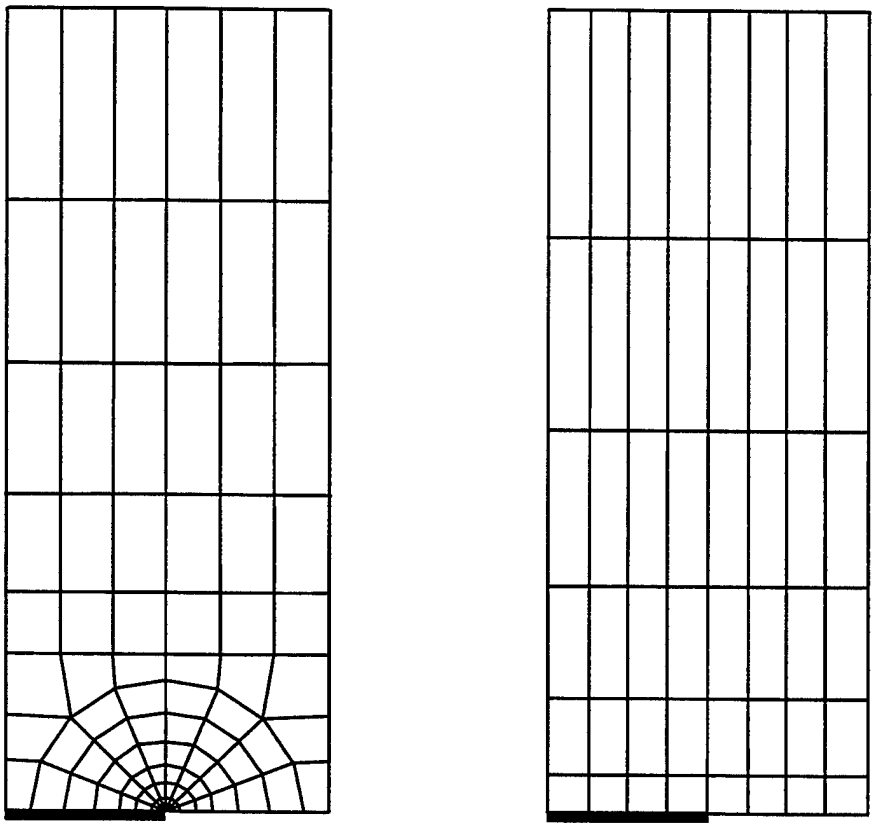

Figure 10: The Finite Element Mesh When a) The EDI Method is Used; b) The Finite Element Alternating Method is Used

using the solution for a single crack in an infinite domain (see the Appendix for theoretical details). With the solution for multiple cracks in an infinite domain, the FEAM can be used to solve problems of multiple cracks with arbitrary crack lengths and orientations at arbitrary locations. This is particularly useful in the treatment of Widespread Fatigue Damage (WFD).

3.2.2 Hybrid Crack-Tip Finite Elements for Modeling Skin-Crack Turning at Stiffeners: Tensile Loading

In assessing the integrity of a structure containing a crack, accurate evaluation of fracture parameters (i.e. stress intensity factors) is required. If the finite element method is used for such purposes, proper numerical modeling of the crack-tip singularities is necessary. An alternative to the Finite Element Alternating Method is to use singular/hybrid crack-tip finite elements. The use of these special elements enables one to use a relatively coarse

finite element mesh around the crack tips; as compared to the very fine and focused mesh when ordinary, non-singular finite elements are used. However, explicit crack-tip meshing must still be carried out and hence this method requires considerable human effort in the construction of meshes as compared to the FEAM.

The hybrid crack element can be used to analyze general anisotropic materials. Hybrid multilayer elements [Nishioka and Atluri(1980)] can be used to study complex, non-self-similar crack growth in composite structures. While self-similar crack growth in a homogeneous anisotropic sheet, can be studied easily using the FEAM, the FEAM cannot be applied to non-self-similar crack growth. Thus the hybrid crack element will be used in the SBIR project to handle problems involving non-self-similar crack growth. In hybrid multilayer elements, the fully three dimensional stress-state, including σ_{33} is accounted for. The mixed-mode stress and strain singularities whose intensities vary within each layer (or a group of layers in a repeated lay-up sequence) near the crack-front, are built into the formulation *a priori*. The interlayer traction reciprocity conditions are satisfied through the use of Lagrange multipliers and individual cross-sectional rotations of each layer are allowed.

In aircraft design, the problem of crack-turning near a stiffener is of particular interest. This is desirable in most situations as it acts as a form of crack arrest. In fact, most aircraft structures are designed with this fail safe feature. The analysis of crack turning at a stiffener will be handled in the damage tolerance module by using the hybrid crack-tip element method. If a crack approaches the stiffener at right angles, the T-stress at the crack tip plays an important role in postulating a criterion which will predict whether the crack will turn along the stiffener. During the process of crack-turning, the hybrid crack elements will be used near the tip of the curving crack, to evaluate the condition for the continued turning of the crack. A constraint based on the T-stress at the crack tip will be introduced in order to account for this crack-turning criterion in the ASTROS design iteration.

3.2.3 Finite Element Alternating Method for Modeling Single or Multiple Part Elliptical Surface Flaws at Holes or Other Stress Raisers: Tensile Loading

The Finite Element Alternating Method for through skin cracks has already been described. The application of the FEAM to surface cracks is similar. In the FEAM for a surface crack in a finite solid, two solutions are required. Solution 1: A general analytical solution for an embedded elliptical crack in a body subject to arbitrary crack face tractions [Vijayakumar and Atluri (1981)].

Solution 2: A numerical scheme (the finite element method in this instance) to solve for the stresses in an uncracked finite body. The analytical solution is for a crack of elliptical shape. Because of this, all physical cracks that are being analyzed must be either elliptical or part elliptical in shape.

The finite element solution involves the analysis of the uncracked solid. Thus, non-zero stresses are calculated at the location of the actual crack. These stresses must be removed in order to create a traction free crack as in the actual problem. The infinite body with an

embedded crack has a solution which is valid for an arbitrary distribution of tractions on the crack face. The detailed steps involved in the FEAM for a crack in a finite body are as follows.

1. Solve the uncracked finite body under the given external loads using the finite element method. The uncracked body has the same geometry as in the given problem except for the crack. For example, when a crack emanates from a hole in a structure, the hole must still be analyzed in the uncracked structure.

2. Using the finite element solution, the program computes the stresses at the crack location.

3. It then compares the residual stresses calculated in Step 2 with a permissible stress magnitude.

4. The residual stresses at the crack location as computed in Step 2 are reversed to create the traction free crack faces as in the given problem. From this, the program determines a polynomial form for these stresses using a "least squares fit".

5. The analytical solution to the infinite body problem with the crack subject to the polynomial loading calculated in Step 4 is now obtained.

6. The stress intensity factors for the current iteration are then calculated from the analytical solution.

7. The residual stresses on the external surfaces of the body due to the applied loads on the crack faces, are now computed. To satisfy the given traction boundary conditions at the external boundaries, the residual stresses on the external surfaces of the body are reversed and this allows calculation of the equivalent nodal forces.

8. Consider the nodal forces in Step 7 as externally applied loads acting on the uncracked body.

All the steps in the iteration process are repeated until the residual stresses on the crack surface become negligible. It has been observed that this iteration process typically takes three or four steps. The overall stress intensity factor solution is obtained by adding the stress intensity factor solutions for all iterations.

One recent application [O'Donoghue, Atluri and Pipkins (1995)] of the FEAM was to the analysis of fatigue cracking in the lower wing skin of the U.S. Air Force C-141B (Fig. 11). In this application, the growth of corner cracks from the weep holes located in the integral risers of the wing skin was modeled with the FEAM (Fig. 12 and Fig. 13). Fatigue crack growth predictions were made wherein the FEAM was used to generate stress intensity factors which were inturn used in a Forman equation. The load spectrum used was comprised of peak-valley pairs representing 3027 equivalent flight hours. Comparisons with limited test data showed good correlation between the FEAM based fatigue crack growth predictions and the experimental data.

Figure 11: U.S. Air Force C-141B

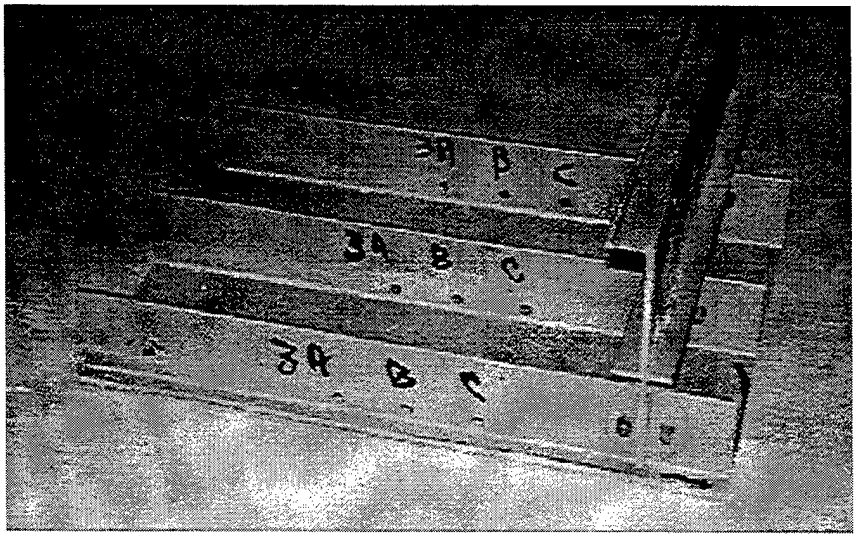

Figure 12: Cut-Out Lower Wing Panel from the C-141B Showing Weep Holes

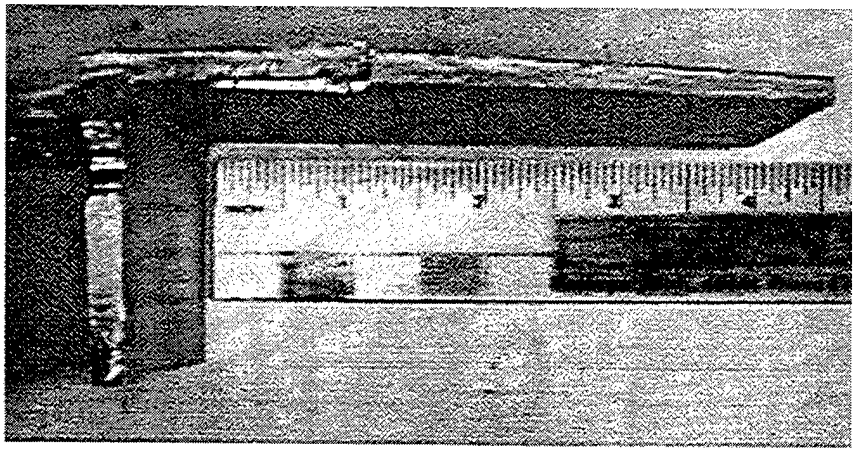

Figure 13: Cross-Section of Failed Lower Wing Panel of the C-141B

3.2.4 Multi-Domain Modeling of the Buckling and Post-Buckling Strengths of Stiffened Panels with Arbitrary Shaped Holes and Delaminations: Compressive Loading

The primary damage in structure loaded in compression which must be considered during design is a hole (Fig. 14). For laminated composites, delaminations will also be of relevance. It is to be expected [with some preliminary results that confirm these expectations being reported in Vellaichamy, et. al (1990)] that the buckling load of a panel, with a hole, in compression will depend on the shape and the size of the hole. The buckling load of a panel with an elliptical hole whose major axis is aligned with the direction of compression can be expected to be lower than that with a circular hole of the same area. Further, it is expected that for an elliptical hole of a given area, the buckling load will decrease with an increase in the aspect ratio of the ellipse, as long as the major axis of the ellipse is aligned with the direction of compression. In the limit as the elliptical hole shrinks to a crack whose axis is parallel to the direction of compression, with the slightest imperfection, the crack may propagate in mode III in post-buckling deformation. Such mode III behavior would severely affect the structural integrity. BUCKDEL, as developed in Phase I of this SBIR project, can be used to compute the buckling and post-buckling response of stiffened structure containing damage in the form of holes and delaminations of arbitrary shape. In addition, it computes the pointwise energy release rate around the delamination front. In future work, the ability to treat the mode III crack problem will be added to BUCKDEL.

A brief overview of BUCKDEL is given here. For more details, see the Users and Theory Manuals which are included with this report. BUCKDEL uses a multi-domain method to model delaminations of arbitrary shape. In this method, the delaminated shell is assumed to be assembled with three regions-(1) Undelaminate: undelaminated zone; (2) Delaminate: thinner side of the delaminated zone and (3) Base: thicker side of the delaminated zone. Transverse shear deformation plays an important part in the case of composite structures,

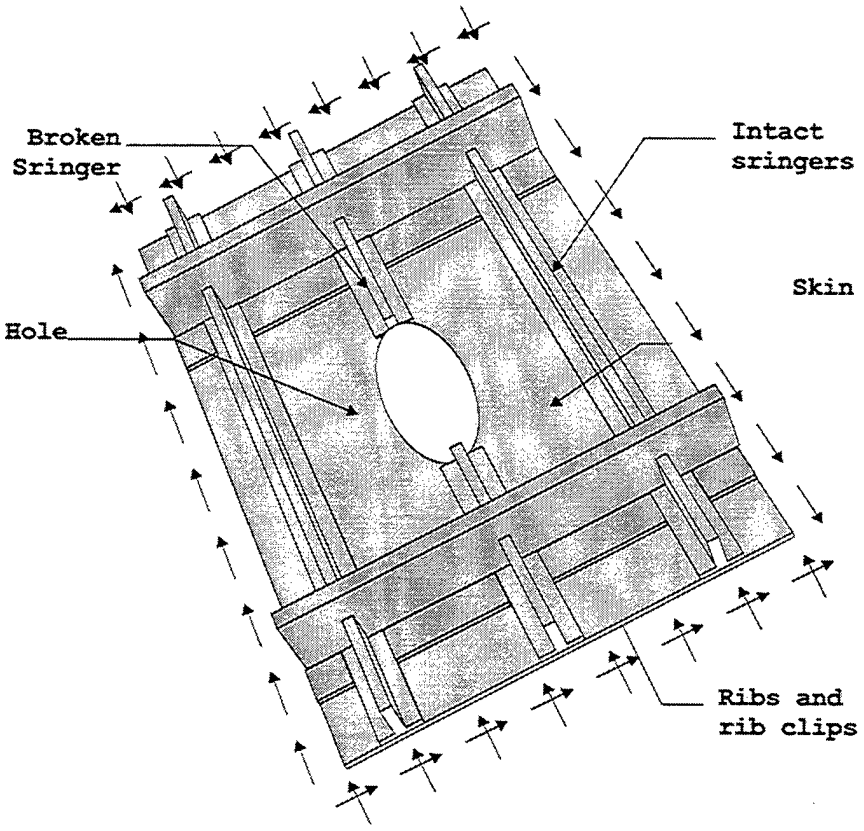

Figure 14: Damage in the Upper (Compression) Skin of a Wing

hence, it is introduced explicitly and the assumptions of Reissner-Mindlin theories of plate bending are used for modeling each region of the multi-domain model. Thus, for each region, the 3-dimensional displacement field ($\mathbf{U} \equiv \{U_1\ U_2\ U_3\}$) is expressed in terms of the corresponding mid-surface displacement ($\mathbf{u} \equiv \{u_1\ u_2\ u_3\}$) and rotation ($\boldsymbol{\theta} \equiv \{\theta_1\ \theta_2\ 0\}$) fields as,

$$\mathbf{U}^{(i)}(x_\alpha, x_3) = \mathbf{u}^{(i)}(x_\alpha) - x_3^{(i)}\boldsymbol{\theta}^{(i)}(x_\alpha) \tag{1}$$

where $x_\alpha^{(i)}$ $(\alpha = 1, 2)$ are the inplane curvilinear shell coordinates and $x_3^{(i)}$ is the thickness coordinate for the i^{th} $(i = 1, 2, 3)$ shell. The structural continuity at the delamination front Γ is maintained by assuming the deformation to be unique at the junction of the three shells i.e. $\mathbf{U}^{(1)} = \mathbf{U}^{(2)} = \mathbf{U}^{(3)}$ on Γ in accordance with the Reissner-Mindlin law of flexure (Eq. (1)). In other words, *at the delamination edge*, the mid-surface degrees of freedom of the delaminate and the base shells are assumed to be related to those of the undelaminated shell by,

$$\left.\begin{array}{ccccc} u_3^{(1)} & = & u_3^{(2)} & = & u_3^{(3)} \\ \theta_\alpha^{(1)} & = & \theta_\alpha^{(2)} & = & \theta_\alpha^{(3)} \\ u_\alpha^{(i)} & = & u_\alpha^{(1)} & + & h^{(i)}\theta_\alpha^{(1)} \end{array}\right)_{at\ \Gamma} \tag{2}$$

where $h^{(i)}$ is the distance of the midsurface of the i^{th} shell from the laminate midsurface.

Each lamina is assumed to be orthotropic and the inplane stresses $\boldsymbol{\sigma}^{(i)} = \{\sigma_{11}\ \sigma_{22}\ \sigma_{12}\}^{(i)}$ and the transverse shear stresses $\boldsymbol{\tau}^{(i)} = \{\tau_{13}\ \tau_{23}\}^{(i)}$ are related to linear components of membrane strain $\boldsymbol{\varepsilon}^{(i)} = \{\varepsilon_{11}\ \varepsilon_{22}\ \varepsilon_{12}\}^{(i)}$; nonlinear components of membrane strain $\boldsymbol{\nu}^{(i)} = \{\nu_{11}\ \nu_{22}\ \nu_{12}\}^{(i)}$; flexural strain due to mid-surface rotation $\boldsymbol{\kappa}^{(i)} = \{\kappa_{11}\ \kappa_{22}\ \kappa_{12}\}^{(i)}$; flexural strain due to transverse shear strain $\boldsymbol{\chi}^{(i)} = \{\chi_{11}\ \chi_{22}\ \chi_{12}\}^{(i)}$ and transverse shear strains $\boldsymbol{\gamma}^{(i)} = \{\gamma_{13}\ \gamma_{23}\}^{(i)}$ as

$$\left\{\begin{array}{c}\boldsymbol{\sigma}\\ \boldsymbol{\tau}\end{array}\right\}^{(i)} = \left[\begin{array}{ccccc} E_{11} & E_{12} & E_{16} & 0 & 0 \\ E_{12} & E_{22} & E_{26} & 0 & 0 \\ E_{16} & E_{26} & E_{66} & 0 & 0 \\ 0 & 0 & 0 & E_{44} & E_{45} \\ 0 & 0 & 0 & E_{45} & E_{55} \end{array}\right]^{(i)} \left\{\begin{array}{c}(\boldsymbol{\varepsilon}+\boldsymbol{\nu}) + x_3\,(\boldsymbol{\kappa}+\boldsymbol{\chi})\\ \frac{1}{2}\boldsymbol{\gamma}\end{array}\right\}^{(i)} \tag{3}$$

where the material constitutive terms $E_{ij}^{(i)}$ are functions of the thickness coordinate of each shell $x_3^{(i)}$. Generally, for a laminate with orthotropic layers, $E_{ij}^{(i)}$ are assumed to be piecewise constants over the laminate thickness.

Integrating along the thickness, the constitutive equations can be written in terms of the inplane stress resultants $\mathbf{N} \equiv \{N_{11}\ N_{22}\ N_{12}\}$, bending moments $\mathbf{M} \equiv \{M_{11}\ M_{22}\ M_{12}\}$, and transverse shear stress resultant $\mathbf{Q} \equiv \{Q_{13}\ Q_{23}\}$, for each region of the multi-plate model as,

$$\left\{\begin{array}{c}\mathbf{N}\\ \mathbf{M}\\ \mathbf{Q}\end{array}\right\}^{(i)} = \left[\begin{array}{ccc}\mathbf{A} & \mathbf{B} & \mathbf{0}\\ \mathbf{B} & \mathbf{D} & \mathbf{0}\\ \mathbf{0} & \mathbf{0} & \mathbf{G}\end{array}\right]^{(i)} \left\{\begin{array}{c}(\boldsymbol{\varepsilon}+\boldsymbol{\nu})\\ (\boldsymbol{\kappa}+\boldsymbol{\chi})\\ \boldsymbol{\gamma}\end{array}\right\}^{(i)} \tag{4}$$

where

$$(A_{kl};\ B_{kl};\ D_{kl})^{(i)} = \int_{t_i} E_{ij}^{(i)}(x_3)\left(1;\ x_3;\ x_3^2\right) dx_3$$

$$G^{(i)}_{mn} = \int_{t_i} s_m s_n E^{(i)}_{ij}(x_3) dx_3$$

In addition to a beam element, BUCKDEL implements a three noded triangular curved shell element. The shell element is described in the curvilinear coordinate system $x-y$ and the area coordinates are used for field-description. Accordingly we have,

$$\{x \;\; y \;\; 1\} = \sum_{i=1}^{3} L_i \{x \;\; y \;\; 1\}_i \tag{5}$$

Inverting the above relationship, we get,

$$L_i = \frac{1}{2\Delta}\left(a_{i1}x + a_{i2}y + a_{i3}\right) \tag{6}$$

where

$$a_{i1} = y_j - y_k; \quad a_{i2} = x_k - x_j; \quad a_{i3} = x_j y_k - x_k y_j$$

$$\Delta = \frac{1}{2}\left(x_2 y_3 - x_3 y_2 + x_3 y_1 - x_1 y_3 + x_1 y_2 - x_2 y_1\right)$$

and $j = 2, 3, 1; \;\; k = 3, 1, 2$ as $i = 1, 2, 3$.

The inplane displacements and the transverse shear strains need to satisfy C^0-continuity while the transverse deflection need to satisfy C^1-continuity in the present formulation. The independent field variables u, v, w, γ_{xz} and γ_{yz} are expressed in terms of the nodal degrees of freedom u_i, v_i, w_i, $\varrho_{x_i} \equiv (-w_{,y})_i$, $\varrho_{y_i} \equiv (w_{,x})_i$, γ_{xz_i} and γ_{yz_i} as,

$$\begin{aligned} \{u \; v \; \gamma_{xz} \; \gamma_{yz}\} &= \sum_{i=1}^{3} L_i \{u \; v \; \gamma_{xz} \; \gamma_{yz}\}_i \\ w &= \sum_{i=1}^{3} \left(N_{1i} w_i + N_{2i} \varrho_{x_i} + N_{3i} \varrho_{y_i}\right) \end{aligned} \tag{7}$$

where

$$\begin{aligned} N_{1i} &= L_i + L_i^2 L_j + L_i^2 L_k - L_i L_j^2 - L_i L_k^2 \\ N_{2i} &= a_{k1}\left(L_i^2 L_j + \frac{1}{2} L_i L_j L_k\right) + a_{j1}\left(L_i^2 L_k + \frac{1}{2} L_i L_j L_k\right) \\ N_{3i} &= a_{k2}\left(L_i^2 L_j + \frac{1}{2} L_i L_j L_k\right) + a_{j2}\left(L_i^2 L_k + \frac{1}{2} L_i L_j L_k\right) \end{aligned} \tag{8}$$

are the cubic polynomials for the transverse deflection.

In the above element formulations, the inter-element C^0-continuity is exactly satisfied for all the field variables. However, the inter-element C^1-continuity required for the transverse deflection, in case of shell element, is satisfied *a posteriori* in a weak form using the Hu-Washizu variational principle.

BUCKDEL uses an automated method to follow the post-buckling paths of the damaged structure. Automated post-buckling solution involves: detection of possible instability in solution and elimination of possible path-retracing; classification of the detected instabilities; and computation of the post-through buckling solution(s). Solution instabilities are detected by monitoring the rank of the tangent stiffness matrix. Whenever the determinant of the tangent stiffness matrix changes its sign the solution senses possible instabilities in that range of load and changes the sign of the next load increment to avoid path-retracing. Through a cycle of iterations, location of instabilities are identified as the load levels for which the tangent stiffness becomes singular. The tangent stiffness is often *scaled* to minimize numerical errors. The identified instability points are then classified as limit points or bifurcation points using some simple and cost-effective rules [Huang and Atluri (1995)]. If the instability point is a limit point, the *arc-length continuation* is enough to obtain post-buckling solution path. However, if the instability point happens to be a bifurcation point, the strategies described in detail in Huang and Atluri (1995) are used to trace the appropriate post-buckling solution branch. The nonlinear fundamental state between the two solution points $n-1$ and n in the neighborhood of the bifurcation point is *linearized* to obtain the *asymptotic* solution for obtaining an approximate critical buckling load factor. A linear combination of the *normalized* eigen-vector associated with the critical buckling load factor and its orthogonal counterpart is used to used to determine the initial post-buckling paths.

3.2.5 Look Up Tables

The finite element based methodologies for modeling the various types of damage being considered in this project are quite general (i.e. they are applicable to complex structural geometries and metallic and composite materials). They are also computationally efficient and very accurate. Nevertheless, it is sometimes useful to have access to cataloged solutions (i.e. stress intensity factors, energy release rates, etc.), which can be used to obtain estimates of the residual strength and life of common structural geometries. In addition to saving computational time, these 'look up' tables can be used to provide sanity checks on the finite element calculations. There are existing programs which are essentially 'look up' tables of stress intensity factors and material property data. Two such programs are AFGROW (formally MODGRO) and NASGRO. It is not the intent of the present project to duplicate effort already expended on programs such as AFGROW and NASGRO. Rather, some of the more common damage scenarios such as the center cracked panel, corner crack at a hole, etc. will be added to the damage tolerance module. By doing so, the user of the damage tolerance module will be able to access parameters such as stress intensity factors for these common damage scenarios without having to go through a finite element analysis. Besides stress intensity factor solutions for structures containing cracks, buckling loads for structures with holes of various sizes and shapes will be available to the user through the 'look up' tables.

3.2.6 Fatigue Crack Growth

The problem of fatigue crack growth is of considerable practical importance when designing a structure which satisfies the DTR. To successfully employ damage tolerance principles, an accurate determination is required of the number of load cycles to failure in a component. These estimates will have a significant influence in the design and maintenance of a safe structure such as in the scheduling of inspection intervals.

Fatigue crack growth frequently occurs when a flawed component is subject to some form of cyclic loading. Here the crack growth is termed subcritical since, due to the cyclic loading, it takes place at stress intensity factor levels that are less than the fracture toughness of the material. The form of the cyclic loading is also of great importance such as whether it has constant amplitude or has a variable amplitude. The damage tolerance module will have the capability to model fatigue crack under conditions of constant amplitude and variable amplitude loading. This capability will be limited to self similar (i.e. Mode I) crack growth.

The crack growth calculations will be performed based on stress intensity factors obtained either by the FEAM or from the 'look up' tables containing cataloged solutions. For reasons of computational efficiency, the 'look up' table method is preferred if a solution is available. For geometries not having cataloged solutions, use will be made of the Finite Element Alternating Method. The FEAM has made the use of finite elements in fatigue calculations feasible. The reason being that the global stiffness matrix of the finite element model is assembled and decomposed only once, since the stiffness of the uncracked structure remains the same for all crack sizes. In other finite element approaches, such as those using singular/hybrid type special crack-tip finite elements or using EDI methods, the cracks must be modeled explicitly. Therefore, the global stiffness matrix must be assembled and decomposed for each crack size. The assembly and decomposition of the global stiffness matrix accounts for about 80% of the computational time required in a typical finite element analysis. Given that the FEAM has to perform this operation only once during a fatigue analysis, the benefits of this approach over other finite element techniques for fatigue crack growth are readily apparent.

Load spectra, in terms of ASTROS load cases, will be provided to the damage tolerance module by the USAGE module described in Nees (1995). Since the USAGE module defines aircraft maneuvers in terms of ASTROS load cases, the load spectra at any point in the aircraft structure can be easily determined by extracting stresses at that point from the ASTROS solution database. Use will be made of USAGE features such as repeating and blocking of data to minimize storage and/or computatational requirements of variable amplitude crack growth calculations.

Numerous studies have been conducted on the characteristics of fatigue crack growth. It has been established that when the plastic or inelastic zone in the vicinity of the crack is small, then the stress intensity factor is the governing parameter during crack growth [Paris and Erdogan (1963)]. In general, the crack growth rate is a function of stress intensity factor change, which is given by:

$$\Delta K = K_{max} - K_{min} \tag{9}$$

where K_{max} is the maximum stress intensity factor during the load cycle and K_{min} is the minimum value of the stress intensity factor. Based on the minimum and maximum loads, it is customary to define the parameter R where:

$$R = K_{min}/K_{max} \tag{10}$$

An important point must be made in relation to the functional relationship between the fatigue crack growth rate and the change in stress intensity factor. This crack growth rate function can be partitioned into three separate regions. At low values of ΔK, there is very little crack growth with a negligible crack growth rate. Therefore, it can be stated that there exists a ΔK below which there is no crack growth. This quantity is referred to as the threshold stress intensity factor and is denoted as $(\Delta K)_{th}$. At higher values of ΔK, crack growth takes place. It has been observed experimentally that this curve, relating the crack growth rate, da/dN, to ΔK, is usually linear on a log-log plot and this corresponds to a power law relation between da/dN and ΔK. This is commonly referred to as the Paris relation and is given as [Paris, Gomez and Anderson (1961)]:

$$\frac{da}{dN} = C(\Delta K)^n \tag{11}$$

where a is the crack length and N is the number of load cycles. The quantities C and n are material dependent constants. At higher values of ΔK the stress intensity factor is approaching the fracture toughness of the material, K_c. The crack growth rate will increase significantly, eventually leading to the onset of rapid unstable crack growth

Recognizing that several distinct phases in fatigue crack growth exist, a more general form for the relationship between crack growth rate and stress intensity factor is expressed as:

$$\frac{da}{dN} = \frac{C(1-R)^m(\Delta K)^n\{\Delta K - (\Delta K)_{th}\}^p}{\{(1-R)K_c - \Delta K\}^q} \tag{12}$$

where m, p and q are constants that relate to the particular crack growth relation that is being used. By assigning different values to these quantities some of the well known crack growth relations can be recovered. For example, when $m = p = q = 0$, the Paris relation is obtained. The Forman relation [Forman, Kearney and Engle (1967)], which accounts for high crack growth rates and instability, is recovered by setting $m = p = 0$ and $q = 1$. By setting $p = q = 0$ and $m = (M_w - 1)n$, the Walker relation [Walker (1970)] is derived, where M_w is an exponent in the Walker relation.

With stress intensity factor solutions and a crack growth relation in hand, the ultimate objective of fatigue crack growth calculations, to calculate the number of cycles for a crack to grow by a specified amount, can be carried out. This is done by integrating the growth relation [Equation (11) or (12)]. For example, equation (11) is integrated to give:

$$N = \frac{1}{A}\int_{a_0}^{a_1} \frac{da}{\Delta K^n} \tag{13}$$

where a_0 and a_1 are the initial and final crack lengths. This integration is done numerically by sub-dividing the crack growth distance into a number of intervals and calculating the stress

intensity factor at each interval. A trapezoidal rule is then used to calculate the number of cycles. All of these steps will be carried out automatically by the damage tolerance module.

Self-similar growth of through skin cracks is straightforward to carry out using the above procedure. However, for an elliptical or part elliptical crack since the stress intensity factor distribution is generally not constant along the elliptical crack front, the crack growth rates will not be the same in every direction. Consequently, the shape of the crack will change. It has been often observed in practice that a semi-elliptical surface crack, initially having a small aspect ratio, will have a larger crack growth rate in the minor axis direction. Therefore, in the damage tolerace module crack growth will be based on the extension of the minor axis by a specified amount. The number of cycles for this is then calculated be evaluating the stress intensity factor at each sub-interval as described earlier. The procedure to adjust the major axis length is as follows. Based on the extension of the minor axis in a given interval, an estimate is made of the extension of the major axis. The cycles for crack growth in these two directions are calculated using Equation (13). Since these are different, in general, the crack extension in the major axis direction is adjusted such that the number of cycles is the same for both directions in a given interval. This is done by simple linear interpolation/extrapolation.

3.3 Integration of the Damage Tolerance Module with ASTROS

This section will address the integration of the damage tolerance module into ASTROS. An important point which must be addressed is the level of integration between the damage tolerance module and ASTROS. Here, level of integration refers to the extent to which the damage tolerance module will make use of existing ASTROS modules which handle tasks such as I/O, memory management, large matrix operations, etc. This subject was investigated during Phase I and it was concluded that the damage tolerance module will be designed to run in a 'stand alone' mode or as an analysis module in ASTROS. This conclusion was reached for the following three reasons.

1. From a development standpoint, complete control over the source code is needed. If the software can be compiled and executed independent of ASTROS, this will assist in debugging, verification, and maximization of computational efficiency. Further, future porting and maintenance of the software will be much simpler.

2. For the purposes of commercialization of the software (which is a requirement of Phase II), some potential customers may need only the damage tolerance module and not the global modeling and multidisciplinary design and optimization capabilities of ASTROS. Thus, they may not be willing to pay the extra costs associated with ASTROS just to be able to make use of the damage tolerance module.

3. Nothing is lost by developing the damage tolerance module to run in both a 'stand alone' mode and as an ASTROS analysis module as opposed to being developed to run only with ASTROS.

The software developed in this SBIR project will consist of four components. These are ASTROS, the USAGE module, an interface module and the damage tolerance module. The software architecture is shown schematically in Fig. 15. The ASTROS system will be rebuilt

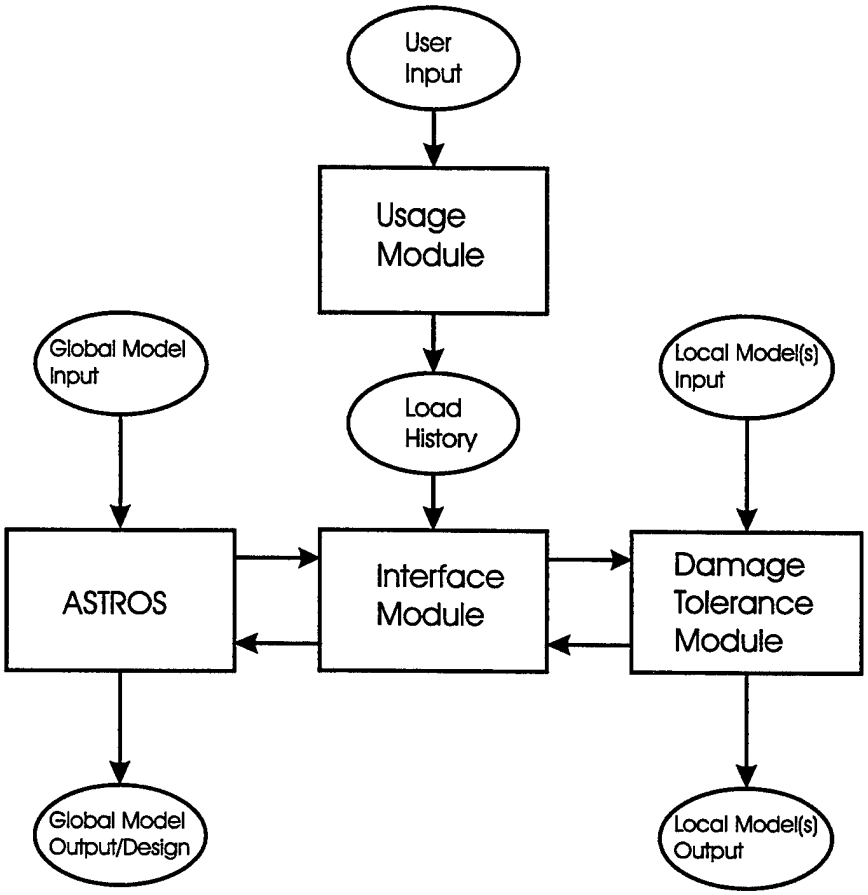

Figure 15: Software Architecture

with a modified MAPOL sequence, new relational entities, new bulk data entities, new error messages and the new module definition so that it will call the damage tolerance module when instructed to do so by the global model input. The USAGE module, described in Nees (1995), will be used to generate load spectra in terms of ASTROS load cases. The interface and damage tolerance module will be coded in FORTRAN 77 by Knowledge Systems. The interface module will facilitate the exchange of data between ASTROS, the USAGE module and the damage tolerance module. The data flowing from ASTROS to the damage tolerance module will be information on the contstraints and associated sensitivities to be evaluated for each local model, current values of the design variables, and boundary conditions to be applied to the local models. The data flowing from the damage tolerance module to ASTROS will be the constraints and sensitivities which were evaluated by the damage module.

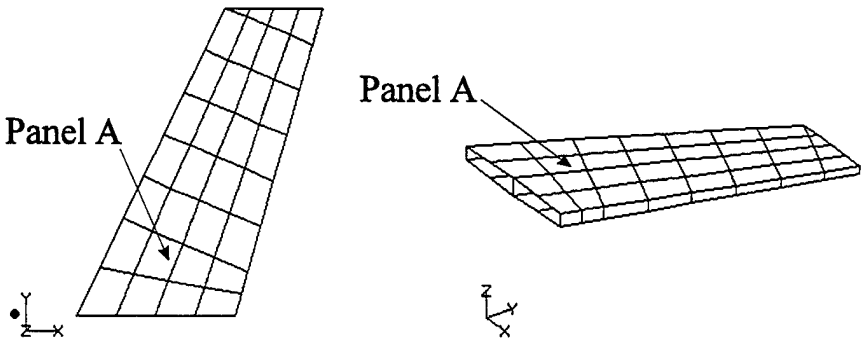

Figure 16: Global Finite Element Model of the Intermediate Complexity Wing (ICW)

3.3.1 Illustration: BUCKDEL Integration with ASTROS

As an explicit illustration of how this integrated system will work, this section describes how the BUCKDEL software [Pipkins and Atluri (1996)], developed in Phase I, would be used to introduce panel buckling constraints, in the presence of delaminations, to the design of the Intermediate Complexity Wing (ICW). In this illustration, BUCKDEL assumes the role of the damage tolerance module of Fig. 15. The ICW model is described in Sections 4.7 and 4.8 of the ASTROS Applications Manual. Fig. 16 shows the global finite element model of the ICW. The model consists of 39 rod elements, 55 shear panel elements, 62 quadrilateral plate elements and 2 triangular plate elements. The substructure material is modeled as aluminum while the wing skins are made of a graphite/epoxy composite. The ICW examples in the ASTROS Applications Manual are designing a minimum weight wing under strength and flutter constraints. In this illustration, panel buckling constraints in the presence of delaminations are also introduced into the design. The panel buckling constraint is applied to Panel A (see Fig. 16). A local finite element model of Panel A (Fig. 17) is developed and will be read as input by BUCKDEL, when it is called by ASTROS.

The integration of BUCKDEL into version 11 of ASTROS is quite easy due to the presence of an existing panel buckling constraint for rectangular panels with no damage. With just a slight modification to the MAPOL sequence, BUCKDEL can be used in place of this panel buckling constraint capability which is included in version 11 of ASTROS. First, the Module Definitions file (MODDEF.DAT) is modified. By doing so, BUCKDEL can then be called by the MAPOL code. Next the MAPOL sequence is edited. MAPOL calls to the engineering application modules PBKLEVAL and PBKLSENS are replaced with calls to BUCKDEL. The arguments passed to and from BUCKDEL would be the same as those passed to and from PBKLEVAL and PBKLSENS except that a flag to inform BUCKDEL whether it is to evaluate a constraint or constraint sensitivity is also passed. With the above changes made to the MODDEF.DAT file and the MAPOL sequence, the SYSGEN program is run. SYSGEN will generate a new XQDRIV subroutine, which provides the

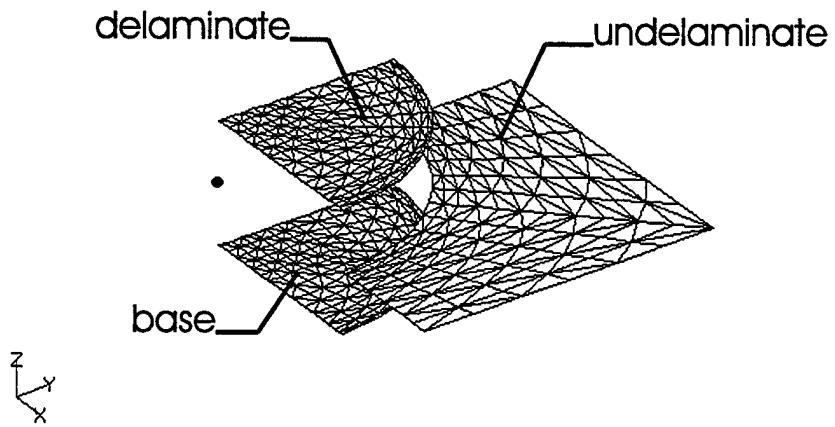

Figure 17: Local Finite Element Model of Panel A with Delamination

actual link between the MAPOL call and the FORTRAN routines that make up BUCKDEL. The new XQDRIV subroutine must be compiled and linked with the ASTROS object file to produce the new executable version of ASTROS which can make use of the damage modeling capabilities in BUCKDEL.

From this point, the use of BUCKDEL to evaluate the panel buckling constraint and associated sensitivities for panel A of the ICW model, with account taken for the presence of a delamination, is exactly the same as the use of the panel buckling constraint capability shipped with version 11 of ASTROS. Namely, the user must specify a DCONBK bulk data card for panel A. After reading the DCONBK bulk data card, ASTROS will call BUCKDEL at the appropriate points in the MAPOL sequence. When called, BUCKDEL will read the local finite element model data for panel A, extract necessary information such as panel loads from the ASTROS database and carry out the constraint or constraint sensitivity evaluation. After evaluating this information, BUCKDEL will store this information in the ASTROS database for use by the optimization routine.

References

[1] Atluri, S.N. (1986) : *Computational Methods in the Mechanics of Fracture.* Amsterdam: North Holland, also translated into Russian, Mir Publishers, Moscow(1989).

[2] Atluri, S. N. (1995) : *Failure Processes in, and Integrity of, Composite Structures; & Life Enhancement of Aging Aircraft*, ICCE/2, Second International Conference on Composite Engineering, Edited by David Hui, August 21-24, 1995, New Orleans, pp. A47-A50.

[3] Atluri, S.N., et. al. (1992): *Composite Repairs of Cracked Metallic Aircraft Structures*, DOT Report No. DOT/FAA/CT-92/32, June 1992.

[4] Britt, V.O. (1994):*Shear and Compression Buckling Analysis for Anisotropic Panels with Elliptical Cutouts* AIAA Journal, Vol. 32, No. 11. pp.551-574.

[5] Brust, F.W.; Atluri, S.N. (1986):*Studies on creep crack growth using the T^* integral.* Engineering Fracture Mechanics, Vol.23, No.3. pp. 2293-2299.

[6] Forman, R.G., Kearney, V.E., Engle, R.M. (1967): *Numerical Analysis of Crack Propagation in Cyclic-Loaded Structures*, Journal of Basic Engineering, v 89, pp. 459-464.

[7] Huang, B-Z.; Atluri, S. N. (1995) : *A simple method to follow post-buckling paths in finite element analysis.* Computers and Structures, v 57, n 3, 477-489

[8] Muskhelishvili, N.I. (1953) : *Some Basic Problems of the Mathematical Theory of Elasticity.* Noordhoo, Groningen.

[9] Nees, C.D. (1995): *Methodology for Implementing Fracture Mechanics in Global Structural Design of Aircraft*, Masters Thesis, Air Force Institute of Technology, Wright-Patterson AFB, OH.

[10] Nemeth, M.P. (1990) : *Buckling and Postbuckling Behavior of Compression-Loaded Isotropic Plates with Cutouts*, AIAA Publication No. AIAA-90-0965-CP, pp. 862-876.

[11] Nishioka, T.; Atluri, S.N. (1980) : *Assumed stress finite element analysis of through-cracks in angle-ply laminates.* AIAA Journal v 18 n 9 1980 p 1125-1132

[12] Nishioka, T.; Atluri, S.N. (1983) : *Analytical solution for embedded elliptical cracks, and finite element alternating method for elliptical surface cracks, subjected to arbitrary loadings.* Eng Fract Mech, v 17 n 3, 1983, p 247-268.

[13] O'Donoghue, P. E.; Nishioka, T.; Atluri, S. N. (1984) : *Multiple surface cracks in pressure vessels.* Eng Fract Mech v 20 n 3 1984 p 545-560

[14] O'Donoghue, P. E.; Nishioka, T.; Atluri, S. N. (1985) : *Multiple coplanar embedded elliptical cracks in an infinite solid subject to arbitrary crack face tractions.* Int J Numer Methods Eng v 21 n 3 Mar 1985 p 437-449

[15] O'Donoghue, P.E.; Atluri, S.N.; Pipkins, D.S. (7995) : *Computational strategies for fatigue crack growth in three dimensions with application to aircraft components.* Eng Fract Mech 52 1 Sept 1995 Pergamon Press Inc Tarrytown NY USA p 51-64

[16] Paris, P.C., Erdogan, F. (1963): *A Critical Analysis of Crack Propagation Laws*, Journal of Basic Engineering, v 85, pp. 528-534

[17] Paris, P.C., Gomez M.P., Anderson W.E. (1961): *A Rational Analytic Theory of Fatigue*, The Trend in Engineering, v 13, pp. 9-14

[18] Park, J.H.; Atluri, S.N. (1993) : *Fatigue growth of multiple-cracks near a row of fastener-holes in a fuselage lap-joint.* Computational Mechanics v 13 n 3 Dec 1993. p 189-203.

[19] Pipkins, D.S.; Atluri, S.N. (1996) : *BUCKDEL v0.9 Users and Theory Manuals* Wright Laboratory Technical Report No. WL-TR-96-xxx.

[20] Vellaichamy, S., Prakash, B.G., and Brun, S. (1990) : *Optimum Design of Cutouts in Laminated Composite Structures,* Computers & Structures, Vol. 37 No. 3, pp. 241-246.

[21] Vijayakumar, K.; Atluri, S.N. (1981) : *An embedded elliptical crack, in an infinite solid, subjected to arbitrary crack-face tractions.* J Appl Mech Trans ASME v 103 n 1 Mar 1981 p 88-96

[22] Walker, K. (1970): *The Effect of Stress Ratio During Crack Propagation and Fatigue for 2024-T3 and 7075-T6 Aluminum,* in Effects of Environment and Complex Load History on Fatigue Life, ASTM STP 462, published by the American Society for Testing and Materials, pp. 1-14.

[23] Wang, L.H.; Atluri, S.N. (1995) : *Implementation of the Schwartz-Neumann alternating method for collinear multiple cracks with mixed type of boundary conditions.* Comput Mech v 16 n 4 p 266-271

[24] Wang, L.H.; Atluri, S.N. (1996) : *Recent advances in the alternating method for elastic and inelastic fracture analyses.* To appear.

[25] Wang, L.H.; Brust, F.W.; Atluri, S.N. (1995a) : *The elastic-plastic finite element alternating method (EPFEAM) and the prediction of fracture under WFD conditions in aircraft structures. Part I. EPFEAM theory.* FAA Center of Excellence Report, August, 1995.

[26] Wang, L.H.; Brust, F.W.; Atluri, S.N. (1995b) : *The elastic-plastic finite element alternating method (EPFEAM) and the prediction of fracture under WFD conditions in aircraft structures. Part II. Fracture and the T^*-integral parameter.* FAA Center of Excellence Report, August, 1995.

[27] Wang, L.H.; Brust, F.W.; Atluri, S.N. (1995c) : *The elastic-plastic finite element alternating method (EPFEAM) and the prediction of fracture under WFD conditions in aircraft structures. Part III. Computational Predictions of the NIST multiple site damage experimental results.* FAA Center of Excellence Report, August, 1995.

Appendix A: Schwartz-Neumann Alternating Method

The Schwartz-Neumann alternating method is based on the superposition principle. The solution on a given domain is the sum of the solutions on two other overlapping domains, with part of the boundary conditions as unknowns. The alternating method can be viewed as the fixed point iteration scheme used to solve these unknown boundary conditions. Based on this point of view, we can perform a convergence study. The alternating method converges unconditionally when there are only traction boundary conditions specified on the body. The convergence criterion for mixed boundary value problems, where there are applied displacement boundary conditions as well as traction boundary conditions, is discussed in the following. Compare the work done by the applied forces in the following two cases. In the first case, arbitrary displacement conditions exist on the surfaces of the cracks in the cracked finite body, while all the boundary conditions elsewhere are replaced by homogeneous boundary conditions, i.e. remove all tractions and reduce all the applied displacements to zero magnitude. In the second case, the same displacement conditions exist on the surfaces of the cracks in the infinite domain. If the work done in the cracked finite body is always smaller than twice of the work done in the infinite domain, the alternating method converges. Otherwise, it does not. For most practical problems, this ratio is close to one. Thus, the alternating method converges rapidly, as discussed in detail in the following section.

A.1 Superposition Principle and the Alternating Method

Consider n cracks in a body of a finite size. The crack surfaces which are traction free, are denoted collectively as Γ_c. Let the boundary of the finite domain(not including the crack surface) be Γ, of which the boundary with prescribed tractions $\boldsymbol{t}^o$ is Γ_t, and the boundary with prescribed displacements $\boldsymbol{u}^o$ is Γ_u. It is clear that $\Gamma = \Gamma_u \cup \Gamma_t$.

The alternating method uses the following two simpler problems to solve the original one. The first one, denoted as P_{ANA} [shown[1] in Fig. 18(c)], is that of the same n cracks in the infinite domain subjected to the unknown crack surface loading $\boldsymbol{T}$. The second one, denoted as P_{FEM} [shown in Fig. 18(b)], has the same finite geometry as in the original problem except that the cracks are ignored. The boundary Γ_u of P_{FEM} has the prescribed displacement $\boldsymbol{u}$, while the boundary Γ_t has the prescribed traction $\boldsymbol{t}$. The prescribed displacements and tractions are different from those in the original problem in general. Because of the absence of the cracks, the problem P_{FEM} can be solved much easier by the finite element method (or the boundary element method).

To solve the original problem, P_{ORG} (shown in Fig. 18(a)), the crack surface loading $\boldsymbol{T}$, the prescribed displacement $\boldsymbol{u}$ and the traction $\boldsymbol{t}$ must be found such that the superposition of the two alternative problems P_{ANA} and P_{FEM} yields the original one, P_{ORG}. The detailed procedures to find these boundary conditions are described as the following.

In the uncracked body problem P_{FEM}, the tractions $\boldsymbol{T}$ at the location of the cracks in

[1]Fig. 18 only illustrates one crack. Many cracks may be present.

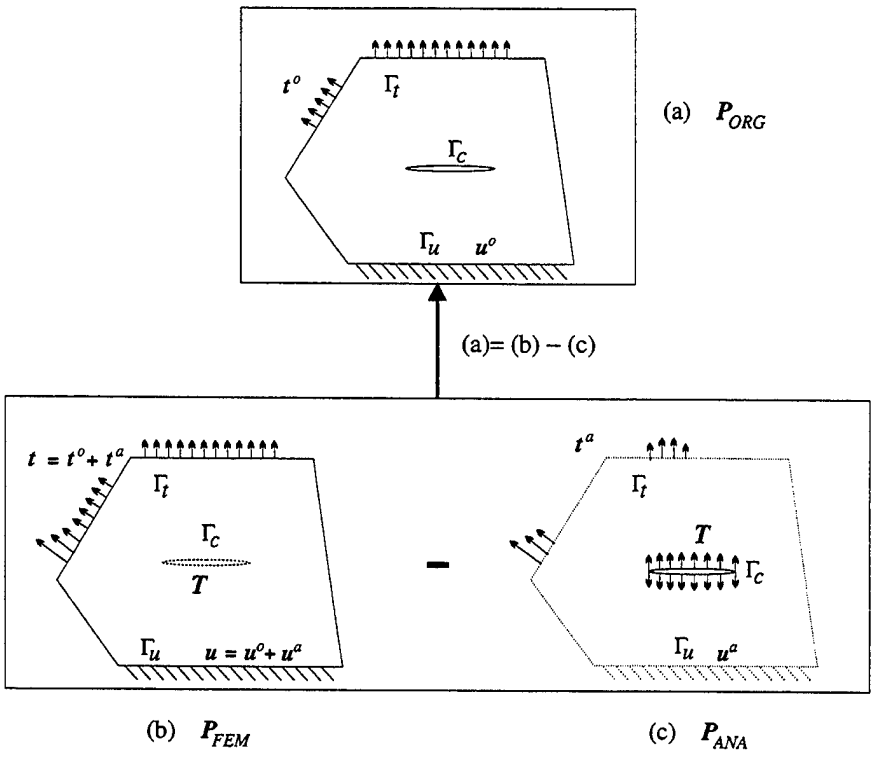

Figure 18: Superposition Principle for Finite Element Alternating Method

the cracked body P_{ORG} can be solved, for any given boundary loads $\boldsymbol{u}$ and $\boldsymbol{t}$, using the finite element method. Due to the linearity of the problem, the solution can be denoted as

$$\boldsymbol{T} = \boldsymbol{K}^u \boldsymbol{u} + \boldsymbol{K}^t \boldsymbol{t} \tag{14}$$

where $\boldsymbol{K}^u$ and $\boldsymbol{K}^t$ are linear operators.

Similarly, the tractions $\boldsymbol{t}^a$ on boundary Γ_t and the displacements $\boldsymbol{u}^a$ on boundary Γ_u can be found in the infinite domain P_{ANA} for the given crack surface load $\boldsymbol{T}$, which is the same as the crack surface traction obtained in the P_{FEM}. The solution can be denoted as

$$\boldsymbol{u}^a = \overline{\boldsymbol{K}^u} \boldsymbol{T} \tag{15}$$

$$\boldsymbol{t}^a = \overline{\boldsymbol{K}^t} \boldsymbol{T} \tag{16}$$

where $\overline{\boldsymbol{K}^u}$ and $\overline{\boldsymbol{K}^t}$ are also linear operators. Subtract the solution for P_{ANA} from the one for P_{FEM}. The resulting solution has zero tractions at the location of the crack surfaces. To ensure that the resulting solution has the same boundary conditions on Γ, the Eq. (17) and Eq. (18) must be satisfied.

$$\boldsymbol{u} = \boldsymbol{u}^o + \boldsymbol{u}^a \tag{17}$$

$$\boldsymbol{t} = \boldsymbol{t}^o + \boldsymbol{t}^a \tag{18}$$

The unknown tractions $\boldsymbol{T}$, $\boldsymbol{t}$ and unknown displacement $\boldsymbol{u}$ can be solved using these equations [Eq. (14) through Eq. (18)]. Eliminate $\boldsymbol{u}$, $\boldsymbol{u}^a$ and $\boldsymbol{t}$, $\boldsymbol{t}^a$ by substituting Eq. (17),

Eq. (18), Eq. (15) and Eq. (16) into Eq. (14) to obtain the following equation for the traction $\boldsymbol{T}$.

$$\left[\boldsymbol{I} - \left(\boldsymbol{K}^u\overline{\boldsymbol{K}^u} + \boldsymbol{K}^t\overline{\boldsymbol{K}^t}\right)\right]\boldsymbol{T} = \left(\boldsymbol{K}^u\boldsymbol{u}^o + \boldsymbol{K}^t\boldsymbol{t}^o\right) \tag{19}$$

Eliminate $\boldsymbol{u}^a$, $\boldsymbol{t}^a$ and $\boldsymbol{T}$ to obtain the following equation for the unknown traction $\boldsymbol{t}$ and unknown displacement $\boldsymbol{u}$.

$$(\boldsymbol{I} - \boldsymbol{A})\left\{\begin{array}{c}\boldsymbol{u}\\ \boldsymbol{t}\end{array}\right\} = \left\{\begin{array}{c}\boldsymbol{u}^o\\ \boldsymbol{t}^o\end{array}\right\} \tag{20}$$

where

$$\boldsymbol{A} = \left[\begin{array}{cc}\overline{\boldsymbol{K}^u}\boldsymbol{K}^u & \overline{\boldsymbol{K}^u}\boldsymbol{K}^t\\ \overline{\boldsymbol{K}^t}\boldsymbol{K}^u & \overline{\boldsymbol{K}^t}\boldsymbol{K}^t\end{array}\right]$$

and $\boldsymbol{I}$ is the identity operator.

Similarly, we can obtain the following linear system for traction $\boldsymbol{t}^a$ and displacement $\boldsymbol{u}^a$.

$$(\boldsymbol{I} - \boldsymbol{A})\boldsymbol{X} = \boldsymbol{Y} \tag{21}$$

where

$$\boldsymbol{X} = \left\{\begin{array}{c}\boldsymbol{u}^a\\ \boldsymbol{t}^a\end{array}\right\}$$

$$\boldsymbol{Y} = \boldsymbol{A}\left\{\begin{array}{c}\boldsymbol{u}^o\\ \boldsymbol{t}^o\end{array}\right\} = \left[\begin{array}{cc}\overline{\boldsymbol{K}^u}\boldsymbol{K}^u & \overline{\boldsymbol{K}^u}\boldsymbol{K}^t\\ \overline{\boldsymbol{K}^t}\boldsymbol{K}^u & \overline{\boldsymbol{K}^t}\boldsymbol{K}^t\end{array}\right]\left\{\begin{array}{c}\boldsymbol{u}^o\\ \boldsymbol{t}^o\end{array}\right\}$$

It is possible to solve these equations directly to obtain the tractions $\boldsymbol{T}$, $\boldsymbol{t}$ and displacement $\boldsymbol{u}$. But this involves the evaluation of $\boldsymbol{K}^u$ and $\boldsymbol{K}^t$, which requires solving the traction $\boldsymbol{T}$ at the location of the uncracked body subjected to all different loading patterns $\boldsymbol{u}$ and $\boldsymbol{t}$. We have to solve the uncracked body problem a larger number of times, of the same order as that of the total number of degrees of freedom of the boundary nodes, using the finite element method. Thus, it can be very expensive to find $\boldsymbol{X}$ by solving directly the linear system $(\boldsymbol{I} - \boldsymbol{A})\boldsymbol{X} = \boldsymbol{Y}$. A fixed point iteration scheme can be used to solve this linear system. The iterative scheme can be devised as:

$$\boldsymbol{X}^{(i+1)} = \boldsymbol{A}\boldsymbol{X}^{(i)} \qquad i = 0, 1, 2, \ldots, \infty \tag{22}$$

where $\boldsymbol{X}^{(0)} = \{\boldsymbol{u}^o, \boldsymbol{t}^o\}^T$. If this procedure converges, the solution is

$$\boldsymbol{X} = \sum_{i=1}^{\infty} \boldsymbol{X}^{(i)}$$

Since

$$\boldsymbol{A} = \left\{\begin{array}{c}\overline{\boldsymbol{K}^u}\\ \overline{\boldsymbol{K}^t}\end{array}\right\} \cdot \left\{\begin{array}{cc}\boldsymbol{K}^u, & \boldsymbol{K}^t\end{array}\right\}$$

the iterative scheme Eq. (22) is equivalent to the following alternating scheme

$$\boldsymbol{T}^{(i)} = \boldsymbol{K}^u\boldsymbol{u}^{(i)} + \boldsymbol{K}^t\boldsymbol{t}^{(i)} \tag{23}$$

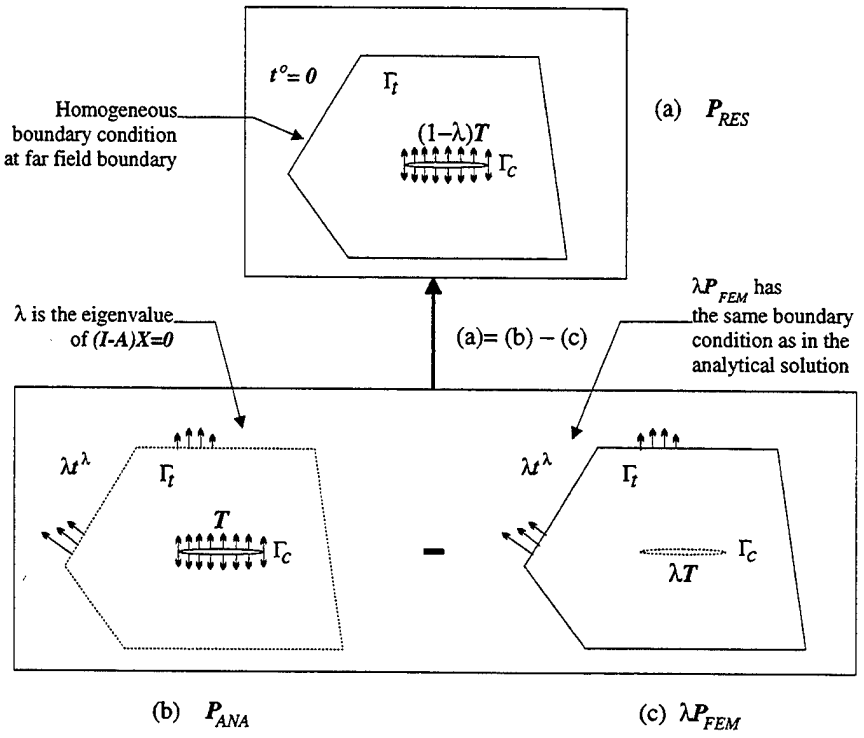

Figure 19: Subtract λP_{FEM} from P_{ANA} to Obtain the Solution for P_{RES} which has Homogeneous Boundary Condition on Γ

$$\left\{ \begin{array}{c} u^a \\ t^a \end{array} \right\}^{(i+1)} = \left\{ \begin{array}{c} \overline{K^u} \\ \overline{K^t} \end{array} \right\} T^{(i)} \tag{24}$$

for $i = 0, 1, 2, \ldots, \infty$. In this case, the uncracked body problem is solved only a few times, because this fixed point iteration scheme converges quickly for practical problems. Therefore, the alternating method is much more efficient than solving the linear system directly. But it should be noticed that it may not be necessary to use the alternating method in some cases. It can be more efficient and accurate to solve directly when multiple crack solutions are constructed from that for a single crack. This will be discussed in detail in a later section.

A.2 Convergence of the Alternating Method

First it is shown that $\boldsymbol{I} - \boldsymbol{A}$ is not singular and the linear system Eq. (21) has a unique solution. Suppose $\boldsymbol{I} - \boldsymbol{A}$ is singular. Then, there must exist a *non-zero* $\boldsymbol{X}$ such that $(\boldsymbol{I} - \boldsymbol{A})\boldsymbol{X} = \boldsymbol{0}$, which means that there exist non-zero $\boldsymbol{u}^a$ and $\boldsymbol{t}^a$, and therefore a non-zero $\boldsymbol{T}$, such that

$$\boldsymbol{T} = \boldsymbol{K}^u \boldsymbol{u}^a + \boldsymbol{K}^t \boldsymbol{t}^a$$

$$\boldsymbol{u}^a = \overline{\boldsymbol{K}^u} \boldsymbol{T}$$

$$\boldsymbol{t}^a = \overline{\boldsymbol{K}^t} \boldsymbol{T}$$

In this case the analytical solution and the finite element solution have the same displacement $\boldsymbol{u}^a$ on boundary Γ_u and the same traction $\boldsymbol{t}^a$ on boundary Γ_t. Subtracting the analytical solution from the FEM solution, we obtain the solution for the following problem. The entire boundary Γ is free of external loadings as well as the crack surfaces. But, the FEM solution gives zero displacements for the crack surfaces, while the analytical solution gives non-zero displacements for the crack surfaces because of the non-zero $\boldsymbol{T}$. Thus, the resulting solution has non-zero displacements at the crack surfaces. This is a contradiction because the cracks cannot be opened without any external load. Consequently, $\boldsymbol{I} - \boldsymbol{A}$ is not singular.

The fixed point iteration scheme Eq. (22) converges if all the eigenvalues of $\boldsymbol{A}$ are in the open interval $(-1, 1)$. The scheme of Eq. (22) converges since the eigenvalues of $\boldsymbol{A}$ are in $(-1, 1)$ for most problems of practical interest. The eigenvalues of $\boldsymbol{A}$ are smaller than 1. Let $\boldsymbol{X}_\lambda$ be an eigenvector of $\boldsymbol{A}$ corresponding to the eigenvalue λ.

$$\boldsymbol{T} = \boldsymbol{K}^u(\boldsymbol{u}^\lambda) + \boldsymbol{K}^t(\boldsymbol{t}^\lambda)$$
$$\lambda \boldsymbol{u}^\lambda = \overline{\boldsymbol{K}^u}\boldsymbol{T}$$
$$\lambda \boldsymbol{t}^\lambda = \overline{\boldsymbol{K}^t}\boldsymbol{T}$$

The solution P_{RES}, shown in Fig. 19(a), is obtained by subtracting λ times the FEM solution(Fig. 19(c)) from the analytical solution(Fig. 19(b)). Here, $\boldsymbol{u} = \boldsymbol{0}$ and $\boldsymbol{t} = \boldsymbol{0}$ on Γ and the crack surface loading is $(1 - \lambda)\boldsymbol{T}$, while the displacements at the crack surfaces are the same as those in the analytical solution. If the work done in opening the cracks in the infinite domain is W, the work done in opening the cracks in the finite domain(with the boundary condition $\boldsymbol{u} = \boldsymbol{0}$ and $\boldsymbol{t} = \boldsymbol{0}$) is $(1 - \lambda)W$, which is equal to the strain energy stored in the body. It must be positive. Thus, $\lambda < 1$.

It can be shown that $\lambda \geq 0$ in the absence of the prescribed displacement boundary conditions. In this case, the resulting solution from the subtraction has zero tractions at the boundary Γ. Apply additional load $\lambda \boldsymbol{t}$ to the boundary Γ with the crack surfaces fixed. The stress state in the body will be the same as that in the analytical solution described above, after this additional loading is applied. This procedure of adding load on the boundary Γ is exactly the same as that in the FEM solution for the uncracked body, except that the load level is λ times of that in the FEM solution, because the crack surfaces are fixed. Therefore, the work done by the additional load is positive. Consequently, $(1 - \lambda)W < W$ and $\lambda > 0$. So, the alternating method converges for cracks in finite domains with arbitrary shapes and arbitrary *traction* boundary conditions.

In general, the eigenvalue λ can be smaller than zero for mixed boundary problems. It is greater than -1 only if $(1-\lambda)W < 2W$. Thus, the convergence criterion for the alternating method for the general case with *mixed* boundary conditions can be stated as follows. The alternating method [Eq. (22)] converges if the crack surface loads do less work in the finite domain, with the homogeneous boundary condition $\boldsymbol{u} = \boldsymbol{0}$ and $\boldsymbol{t} = \boldsymbol{0}$ on Γ, than twice as much as they do in the infinite domain for *any* arbitrary distribution of crack surface displacements (see Fig. 20).

Quick convergence can be expected for most of the practical applications. For any crack surface displacements, the displacements and stresses at a point decay rapidly as the point

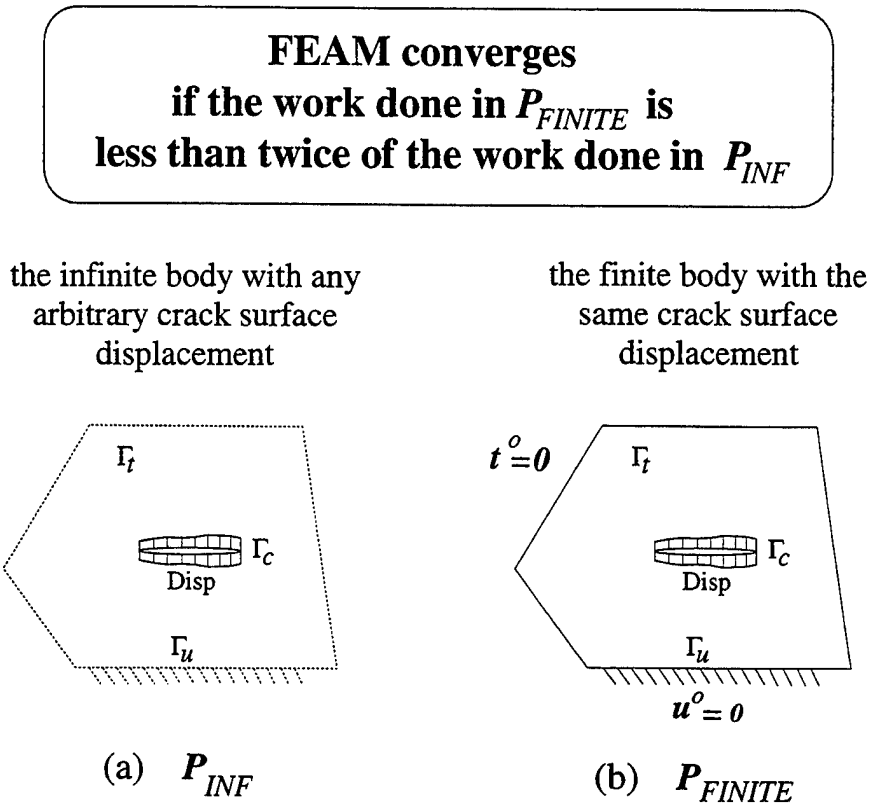

Figure 20: Convergence Criterion

moves away from the cracks. Thus, the work done in the finite domain with the homogeneous boundary condition is very close to the work done in the infinite domain. This implies that the eigenvalues of $\boldsymbol{A}$ are very small and the fixed point iteration converges rapidly. Indeed, all mixed boundary value problems we have solved (for both 2D and 3D problems) to date using finite element alternating method have converged.

A.3 Summary of FEAM Procedure

The alternating procedure defined in Eq. (22) can be translated into the following simple procedure. Refer to Fig. 18.

1. Solve P_{FEM} with the given load on the boundary Γ. Solve for the tractions, which are used to close the cracks. Denote the solution as S_1^{FEM}, where 1 indicates that this is the solution for the first iteration.

$$S_1^{FEM}: \quad \boldsymbol{T}^{(1)} = \boldsymbol{K}^u \boldsymbol{u}^o + \boldsymbol{K}^t \boldsymbol{t}^o$$

2. *Reverse* the crack surface traction obtained in the previous step and apply it as the load on the crack surfaces and solve the P_{ANA}. Denote the solution as S_1^{ANA}.

$$-S_1^{ANA}: \quad \left\{ \begin{array}{c} \boldsymbol{u} \\ \boldsymbol{t} \end{array} \right\}^{(1)} = \left\{ \begin{array}{c} \overline{\boldsymbol{K}^u} \\ \overline{\boldsymbol{K}^t} \end{array} \right\} \boldsymbol{T}^{(1)}$$

3. Find the tractions on the boundary Γ_t and the displacements on the boundary Γ_u from the analytical solutions obtained in the previous step. *Reverse* them as the load for P_{FEM}. Find the crack closing tractions from the solution S_2^{FEM}.

$$S_2^{FEM}: \quad \boldsymbol{T}^{(2)} = \boldsymbol{K}^u \boldsymbol{u}^{(1)} + \boldsymbol{K}^t \boldsymbol{t}^{(1)}$$

4. Repeat the step 2 and 3 until the residual load is small enough to be ignored.

$$-S_i^{ANA}: \quad \left\{ \begin{array}{c} \boldsymbol{u} \\ \boldsymbol{t} \end{array} \right\}^{(i)} = \left\{ \begin{array}{c} \overline{\boldsymbol{K}^u} \\ \overline{\boldsymbol{K}^t} \end{array} \right\} \boldsymbol{T}^{(i)}$$

$$S_{i+1}^{FEM}: \quad \boldsymbol{T}^{(i+1)} = \boldsymbol{K}^u \boldsymbol{u}^{(i)} + \boldsymbol{K}^t \boldsymbol{t}^{(i)}$$

for $i = 2, 3, \ldots$.

The solution to the original problem is the summation of all those obtained in the alternating procedure, i.e.

$$S = \sum_{i=1}^{n} \left(S_i^{FEM} + S_i^{ANA} \right) \tag{25}$$

A.4 Solutions for Multiple Skin Cracks

Solutions for multiple skin cracks in an infinite body, subjected to arbitrary crack surfaces tractions, can be constructed using the solution for a single crack in a infinite body subjected to arbitrary crack surface loading. Analytical solutions for multiple embedded cracks in an infinite body are available only for some special configurations, such as multiple collinear cracks subjected to arbitrary crack surface tractions [Muskhelishvili (1953)]. There are several implementations of finite element alternating method based on such analytical solutions [Park and Atluri (1993), Wang and Atluri (1995), etc.]. It is in general easier to construct the solution of multiple embedded cracks in an infinite body using the solution for a single embedded crack. Solutions for arbitrary distributions of cracks can be obtained using this approach. It can be more accurate and efficient to build the multiple crack solutions from that for a single crack even when the analytical solution is available, such as for the multiple collinear cracks in an infinite domain.

In the context of the finite element alternating method, it seems natural to use the Schwartz-Neumann alternating method to obtain the analytical solution iteratively. This approach has been used by many authors, such as O'Donoghue, Nishioka and Atluri (1984) and (1985). Using the alternating method and the solution for the single crack in the infinite

domain, residuals induced by closing the other cracks are erased by reversing them and applying them as loads on the crack surfaces. Consider n arbitrarily distributed cracks. Let the given crack surface load on k'th crack be $\boldsymbol{T}_k^o$, $(k = 1, 2, \ldots n)$. The alternating procedure is outlined as the following.

1. Consider a single crack, located at the same position as that of the k'th crack in the original problem, in the infinite domain. Apply the load $\boldsymbol{T}_k^o$ on the crack surface. Denote the analytical solution for this loading as $S_k^{(0)}$.

2. Compute the cohesive traction $\boldsymbol{t}_{jk}^{(0)}$, that is used to close the j'th crack in the original problem, using the solution $S_k^{(0)}$.

$$S_k^{(0)}: \quad \boldsymbol{t}_{jk}^{(0)} = \boldsymbol{K}_j^{[k]} \boldsymbol{T}_k^{(0)} \qquad j = 1, 2, \ldots, n \quad \text{and} \quad j \neq k$$

   where $\boldsymbol{T}_k^{(0)} = \boldsymbol{T}_k^o$, and $\boldsymbol{K}_j^{[k]}$ $(j = 1, 2, \ldots, n$ and $j \neq k)$ are linear operators. The superscript $^{[k]}$ indicates that the crack in the single-crack solution is at the same location as the k'th crack in the original multiple-crack problem.

3. Sum the crack closure tractions due to all solution $S_k^{(0)}$, $(k = 1, 2, \ldots, n)$ to find the residual traction. *Reverse* the residual tractions as loads.

$$\boldsymbol{T}_j^{(1)} = - \sum_{k=1, k \neq j}^{n} \boldsymbol{t}_{jk}^{(0)} \qquad j = 1, 2, \ldots, n$$

4. Apply the load $\boldsymbol{T}_k^{(1)}$ on the crack surface as in the first step. Denote the solution as $S_k^{(1)}$. Repeat the process of finding residual tractions until the residual tractions are small enough to be ignored.

$$S_k^{(i)}: \quad \boldsymbol{t}_{jk}^{(i)} = \boldsymbol{K}_j^{[k]} \boldsymbol{T}_k^{(i)} \qquad j = 1, 2, \ldots, n \qquad j \neq k$$

$$\boldsymbol{T}_j^{(i+1)} = - \sum_{k=1, k \neq j}^{n} \boldsymbol{t}_{jk}^{(i)} \qquad j = 1, 2, \ldots, n$$

   for $i = 1, 2, \ldots$.

The solution to the multiple cracks subjected to the given load $\boldsymbol{T}_k^o$ $(k = 1, 2, \ldots, n)$ is the sum of all the solutions involved in the alternating procedure, i.e.

$$S = \sum_{i=1}^{\infty} \sum_{k=1}^{n} S_k^{(i)}$$

However, the solution can be obtained using a non-iterative approach in a simpler and more efficient fashion. As we have shown in the previous section, an alternating method is essentially a fixed point iteration scheme used to solve a linear system. In the analysis of a

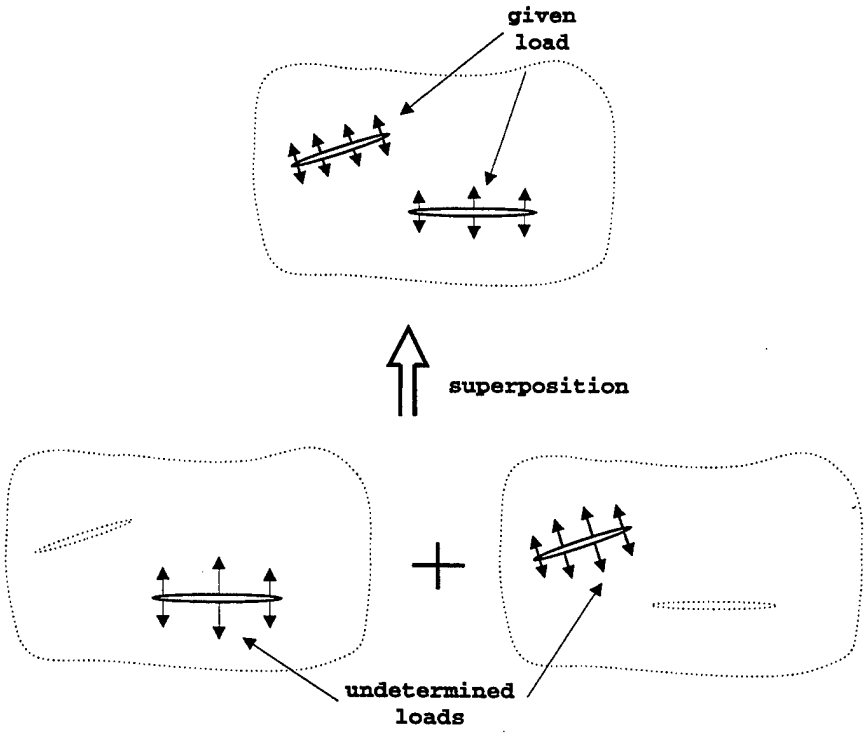

Figure 21: Superpose the Single Crack Solutions

cracked body, solving the linear system directly needs crack closure tractions for all possible boundary loadings. Thus the uncracked body problem has to be solved a large number of times, of the same order as that of the total number of degrees of freedom of the nodes at the boundary, for different loadings. Only a few iterations are needed when finite element alternating method is used. Thus the uncracked body is solved only a few times.

On the other hand, these tractions can be easily evaluated in the analysis of multiple cracks using the analytical solutions. Since the number of degrees of freedom involved is small, the linear system can be solved directly.

The linear system for solving the multiple crack problem is derived from the superposition principle. Consider the superposition of n solutions of single cracks in the infinite body. Each of these n solutions involves only one crack. Denote the k'th solution as S_k, where the crack is at the same location as that of the k'th crack of the original multiple-crack problem. The crack surface traction $\boldsymbol{T}_k$ for the problem S_k $(k = 1, 2, \ldots, n)$ is to be determined(see Fig. 21).

The traction at the location of the j'th crack in the the problem S_k can be found for any load $\boldsymbol{T}_k$, i.e.

$$\boldsymbol{t}_{jk} = \boldsymbol{K}_j^{[k]} \boldsymbol{T}_k \qquad j, k = 1, 2, \ldots, n. \tag{26}$$

It is noticed that $\boldsymbol{K}_k^{[k]} = \boldsymbol{I}$ $(k = 1, 2, \ldots, n)$ are identity operators, because the tractions at the crack surfaces are the same as the applied loads.

The superposition of the n solutions should give back the original problem, i.e. the tractions at the locations of the crack surfaces should be the same as the given crack surface loads. Thus, the linear system to be solved is

$$\sum_{k=1}^{n} \boldsymbol{t}_{jk} = \sum_{k=1}^{n} \boldsymbol{K}_j^{[k]} \boldsymbol{T}_k = \boldsymbol{T}_j^o \qquad j = 1, 2, \ldots, n. \tag{27}$$

We can denote collectively the undetermined crack surface loads, $\boldsymbol{T}_k$ $(k = 1, 2, \ldots, n)$, as $\boldsymbol{T}$. Similarly, denote collectively the given loads, $\boldsymbol{T}_k^o$ $(k = 1, 2, \ldots, n)$, as $\boldsymbol{T}^o$, Thus, Eq. (27) can be rewritten as

$$\boldsymbol{K}\boldsymbol{T} = \boldsymbol{T}^o \tag{28}$$

where $\boldsymbol{K}$ is a linear operator. Once the linear operator $\boldsymbol{K}$ is evaluated numerically, we can solve the linear system directly instead of using alternating method.

Crack surface tractions have to be discretized by a set of linearly independent basis functions, such as polynomial functions, Chebyshev polynomials, or certain piecewise continuous functions, since arbitrary crack surface tractions can not be handled directly by numerical methods.

Let the undetermined load $\boldsymbol{T}$ be approximated by N basis functions $\boldsymbol{B}_j$ $(j = 1, 2, \ldots, N)$.

$$\boldsymbol{T} \approx \sum_{j=1}^{N} T_j \boldsymbol{B}_j \tag{29}$$

Similarly, the given load $\boldsymbol{T}^o$ which can be approximated as in the following.

$$\boldsymbol{T}^o \approx \sum_{i=1}^{N} T_i^o \boldsymbol{B}_i \tag{30}$$

We apply load $\boldsymbol{B}_i$ on the cracks. Close all other cracks except the *single* crack on which $\boldsymbol{B}_i$ has non-zero values. Find the tractions at the locations of the n cracks of the original problem (see[2] Fig. 22), using the analytical solution for a single crack in an infinite domain.

$$\boldsymbol{t}_j = \boldsymbol{K}\boldsymbol{B}_j \qquad j = 1, 2, \ldots, N \tag{31}$$

where $\boldsymbol{K}$ is a linear operator. The tractions $\boldsymbol{t}_j$ $(j = 1, 2, \ldots, N)$ are also approximated by these basis functions.

$$\boldsymbol{t}_j \approx \sum_{i=1}^{N} t_{ji} \boldsymbol{B}_i \qquad j = 1, 2, \ldots, N \tag{32}$$

Once the magnitude t_{ij} are evaluated, the traction at the location of k'th crack can be determined for a crack surface load $\boldsymbol{T}_k$. Since

$$\boldsymbol{t} \;=\; \boldsymbol{K}\boldsymbol{T}$$

[2]Point loads (Delta functions) are used to illustrate the base functions in the figure. Only some of the loading cases are illustrated in the figure.

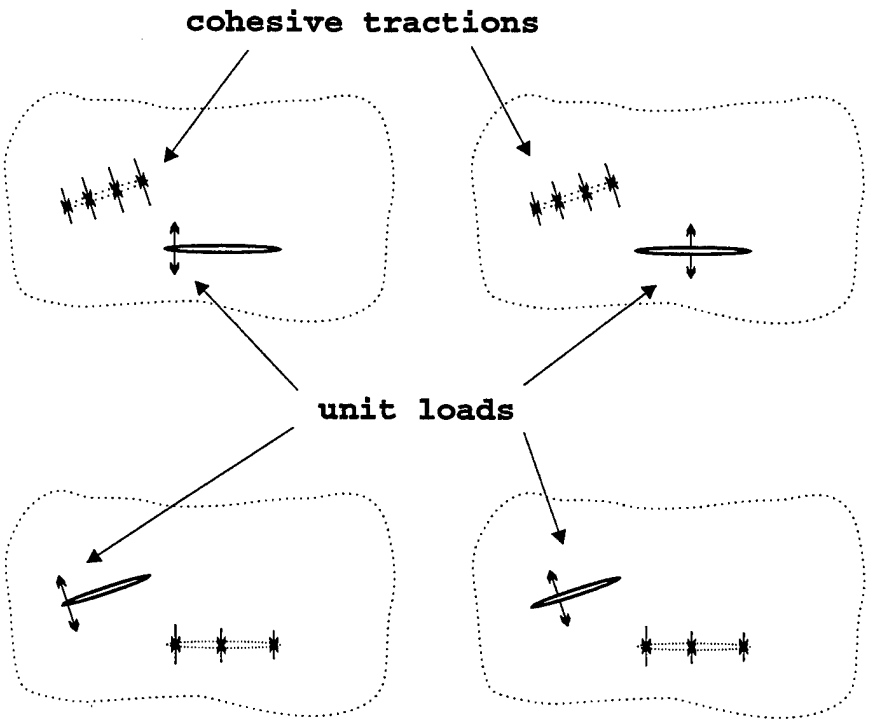

Figure 22: Evaluate the Traction at the Locations of Cracks for Each Load in Terms of Unit Basis Functions

$$\begin{aligned} &\approx \boldsymbol{K}\left(\sum_{j=1}^{N} T_j \boldsymbol{B}_j\right) \\ &= \sum_{j=1}^{N} T_j \boldsymbol{K}\boldsymbol{B}_j \\ &\approx \sum_{j=1}^{N}\sum_{i=1}^{N} t_{ji} T_j \boldsymbol{B}_i \end{aligned}$$

the linear system Eq. (28) can be approximated as

$$\sum_{j=1}^{N}\sum_{i=1}^{N} t_{ji} T_j \boldsymbol{B}_i = \sum_{i=1}^{N} T_i^o \boldsymbol{B}_i \tag{33}$$

which leads to the following linear system of equations for the magnitudes T_j $(j = 1, 2, \ldots, n)$.

$$\sum_{j=1}^{N} t_{ji} T_j = T_i^o \qquad i = 1, 2, \ldots, N \tag{34}$$

The alternating method essentially solves the same approximated linear system with a fixed point iteration scheme.

The non-iterative procedure to solve the multiple crack problem is summarized as the following.

1. Apply loads in terms of unit basis functions on one of the cracks, ignoring the other cracks. Use the analytical solution for a single crack to solve the tractions at the locations of all the other cracks (see Fig. 22).

2. Approximate these tractions in terms of the linear combination of the basis functions. Find the magnitude of each component. Thus, the coefficients of the linear system is determined as in Eq. (32).

3. Approximate the given crack surface load $\boldsymbol{T}_k$ in terms of the linear combination of the basis functions. Find the magnitude of each components.

4. Solve the linear system Eq. (34) to obtain the the loads applied on each single crack solution.

5. Superpose the n single crack solutions to form a solution for the original problem.

The coefficients of the linear system remain the same in the analysis of the same cracks under different loadings, because they depend only on the crack configuration and the basis functions. Thus, the linear system can be solved for different loads without recomputing the coefficients of the system. This feature is particularly useful when the constructed multiple crack solution is used in the finite element alternating method, where it is necessary to evaluate the solution for the same cracks under different loadings during the alternating procedure.